TECHNICAL REPORT RD-SS-88-11

REMARKS ON CERTAIN ASPECTS OF SOLID EXPLOSIVE DETONATION VIA SMALL PROJECTILE IMPACT

James P. Billingsley
Carl L. Adams
Systems Simulation and Development Directorate
Research, Development, and Engineering Center

MAY 1989

U.S. ARMY MISSILE COMMAND
Redstone Arsenal, Alabama 35898-5000

DISPOSITION INSTRUCTIONS

DESTROY THIS REPORT WHEN IT IS NO LONGER NEEDED. DO NOT RETURN IT TO THE ORIGINATOR.

DISCLAIMER

THE FINDINGS IN THIS REPORT ARE NOT TO BE CONSTRUED AS AN OFFICIAL DEPARTMENT OF THE ARMY POSITION UNLESS SO DESIGNATED BY OTHER AUTHORIZED DOCUMENTS.

TRADE NAMES

USE OF TRADE NAMES OR MANUFACTURERS IN THIS REPORT DOES NOT CONSTITUTE AN OFFICIAL INDORSEMENT OR APPROVAL OF THE USE OF SUCH COMMERCIAL HARDWARE OR SOFTWARE.

REPORT DOCUMENTATION PAGE

Form Approved
OMB No 0704-0188
Exp Date Jun 30, 1986

1a. REPORT SECURITY CLASSIFICATION Unclassified	1b. RESTRICTIVE MARKINGS
2a. SECURITY CLASSIFICATION AUTHORITY	3. DISTRIBUTION/AVAILABILITY OF REPORT Approved for public release; distribution is unlimited.
2b. DECLASSIFICATION/DOWNGRADING SCHEDULE	
4. PERFORMING ORGANIZATION REPORT NUMBER(S) RD-SS-88-11	5. MONITORING ORGANIZATION REPORT NUMBER(S)
6a. NAME OF PERFORMING ORGANIZATION Sys Sim & Dev Dir, Res, Dev, & Eng Ctr 6b. OFFICE SYMBOL (If applicable) AMSMI-RD-SS	7a. NAME OF MONITORING ORGANIZATION
6c. ADDRESS (City, State, and ZIP Code) Commander U.S. Army Missile Command ATTN: AMSMI-RD-SS Redstone Arsenal, AL 35898-5270	7b. ADDRESS (City, State, and ZIP Code)
8a. NAME OF FUNDING/SPONSORING ORGANIZATION 8b. OFFICE SYMBOL (If applicable)	9. PROCUREMENT INSTRUMENT IDENTIFICATION NUMBER
8c. ADDRESS (City, State, and ZIP Code)	10. SOURCE OF FUNDING NUMBERS PROGRAM ELEMENT NO. / PROJECT NO / TASK NO / WORK UNIT ACCESSION NO

11. TITLE (Include Security Classification)
Remarks on Certain Aspects of Solid Explosive Detonation via Small Projectile Impact (U)

12. PERSONAL AUTHOR(S)
James P. Billingsley and Carl L. Adams

13a. TYPE OF REPORT	13b. TIME COVERED	14. DATE OF REPORT (Year, Month, Day)	15. PAGE COUNT
FINAL	FROM 07/86 TO 07/88	May 1989	104

16. SUPPLEMENTARY NOTATION

17. COSATI CODES			18. SUBJECT TERMS (Continue on reverse if necessary and identify by block number)		
FIELD	GROUP	SUB-GROUP	Detonation Criteria	Comp-B3	PBX-9404
			Impacted Explosives	Comp-B	Tetryl
			Shocked Explosives	TNT	

19. ABSTRACT (Continue on reverse if necessary and identify by block number)

Criteria for high explosive detonation via projectile impact have important lethality, survivability and safety implications. Five sets of classic projectile impact induced detonation data were reexamined and reevaluated with respect to Moulard's critical area concept. Some empirical relations were found which are simple functions of the critical area or the projectile cross-section area and known impact shock variables. These relations enhance and/or supplement current empirical detonation prediction methodology, and could lead to a better understanding of the underlying physical phenomena.

Furthermore, results from this investigation imply that a minimum (or critical) area dependent shock energy input rate (or power) is necessary for detonation initiation. This minimum amount of power must be sustained for a minimum length of time. This result for solid explosives is analogous to a power input criterion for gaseous explosive detonation which is well documented in the technical literature.
(Continued)

20. DISTRIBUTION/AVAILABILITY OF ABSTRACT	21. ABSTRACT SECURITY CLASSIFICATION	
☐ UNCLASSIFIED/UNLIMITED ☒ SAME AS RPT ☐ DTIC USERS	Unclassified	
22a. NAME OF RESPONSIBLE INDIVIDUAL Dr. James P. Billingsley	22b. TELEPHONE (Include Area Code) (205) 876-5210	22c. OFFICE SYMBOL AMSMI-RD-SS

DD FORM 1473, 84 MAR — 83 APR edition may be used until exhausted. All other editions are obsolete.

Block 19. (Continued)

It is empirically shown that the area dependent energy rate (power) is inversely proportional to the shock velocity in the explosive. For true one-dimensional situations, the area dependent power requirement is indistinguishable from the constant energy (per unit area) criteria.

An important spinoff from this investigation is the formulation of a scheme to predict the minimum shock pressure required to detonate an explosive. This scheme is based on E. R. Fitzgerald's crystal lattice fracture/disintegration criteria. Some pertinent results are given in this report, but the concept and analysis are being documented in a separate publication.

ACKNOWLEDGEMENT

The authors gratefully acknowledge the assistance they have received from Mr. C. James Head, who wrote a computer code to check the tabular results.

TABLE OF CONTENTS

LIST OF ILLUSTRATIONS

LIST OF TABLES

I. INTRODUCTION

Criteria for high explosive detonation via projectile impact are important from both safety and lethality considerations. The study of both impact and explosive detonation encompasses some of the most complex phenomena encountered in the physical sciences. Consequently, each area (high velocity impact and explosive detonation) has been the subject of numerous conferences, symposiums, and technical papers.

Since projectile induced detonation criteria has such important lethality, safety, and survivability implications, a technical literature information search was initiated. A primary objective was to acquire insight into the physical phenomena causing detonation via impact. This, in turn, could lead to better utilization, or even enhancement, of present empirical predictive schemes employed in various lethality codes. Reference 1 employs part of this predictive methodology (the Jacobs-Roslund equation) in the analysis of experimental data.

This information search has yielded five sets of experimental data which have been reexamined in this investigation. These data have been derived by subjecting bare unprotected explosive samples to normal impact of flat-faced projectiles as schematically shown in Figure 1. The basic information, which came from diverse sources, is plotted in Figure 2.

The information search is continuing and appropriate data are being reexamined. However, enough analysis has been done to indicate that enhancements or supplements to certain portions of the current empirical detonation prediction methodology may be feasible or even necessary. In any event, the current methodology (for prediction of explosive detonation via projectile velocity and size) could be checked by incorporating the "critical area" (A_{cr}) concept suggested by Henry Moulard [2] and [3].

Specifically, during the present investigation, some empirical relationships were found which are simple functions of known impact shock variables and either A_{cr} or A, the projectile cross-section area.

These relations, involving cross-section area dimensions, can be useful in projectile size/detonation prediction criteria, for lethality/survivability assessment codes.

Even though the physical meaning of certain empirical relations is not crystal clear, their uniform and consistent data correlation suggests that they are natural parameters associated with fundamental physical phenomena. While searching for some explanation of the strong critical area effect, its connection with an energy rate or power input was found.

The present investigation strongly indicates that a minimum (or critical) area dependent shock energy input rate (or power) is necessary for detonation initiation. This is analogous to results reported by investigators of gaseous explosive detonation. This minimum amount of power input, joules/microsecond (J/μsec), must be sustained for a minimum amount of time (t_{cr}), which is dependent on the overall energy input requirements.

It is shown that the area dependent energy rate is inversely proportional to the shock velocity in the explosive. An obvious question is: "What is the minimum shock velocity required to initiate reactions leading to detonation?" This question led to the results described in Appendix G. In this appendix, a crystal lattice fracture or disintegration criteria is applied to compute the minimum shock velocity and pressure required to initiate detonation. More work remains to be done with respect to this concept, since it appears to be fundamentally significant.

Time wise integration of the area dependent energy input rate expression produced an expression for the total high shock energy input as a function of time. This expression is employed to demonstrate that when the projectile and explosive cross section areas are sufficiently larger than A_{cr}, then the well known (area independent) constant energy per unit area detonation criteria will logically appear as the dominant parameter. This situation is prevalent in the one-dimensional tests and it may obscure the important energy rate (or power) input role.

The seven appendices of this report provide certain background information with respect to:

A, B - Shock Phenomenon and Data

C - The Critical Energy Criteria

D - The Critical Area Criteria

E - Current Projectile Impact Prediction Criteria

F - Explosive Rod Diameter Effect

G - Crystal Lattice Fracture and Detonation Criteria

II. ANALYSIS

A. Critical Area A_{cr} Relations

Moulard [2] clearly demonstrated his point with respect to A_{cr} for an explosive which conformed to the constant energy criteria ($P_s\ U_{p_{ex}}\ t_{cr}$ = Const). The constant energy relation [4] was developed from an examination of one dimensional thin metallic foil planar impact detonation data reported in [5]. Moulard points out that small projectile or fragment impact is a three-dimensional phenomenon, even if the contact surfaces are planar. Moulard showed that a minimum shock loaded interface contact area (A_{cr}) is important in addition to the well known shock pressure (P_s) and duration (t_{cr}) conditions from the constant energy per unit area relation:

$$P_s\ U_{p_{ex}}\ t_{cr} = C_1 = \text{Constant} \tag{1}$$

$U_{p_{ex}}$ = Particle velocity of the explosive behind the shock front.

A dimensional analysis of Eq. (1) reveals that:

$$P_s\ U_{p_{ex}}\ t_{cr} = \left(\frac{F}{L^2}\right)\left(\frac{L}{t}\right)t = \frac{FL}{L^2} = \frac{\text{Work}}{\text{Area}}$$

$$= \frac{F}{L} = \frac{\text{Force}}{\text{Length}} \tag{2}$$

This shows that force per unit length could also be important. Was there some other combination of variables having dimensions of force per unit length which was constant also? Subsequent work with Moulard's [2] data for the Comp-B3 explosive (Table 1 and Appendix D) revealed empirically that:

$$P_s\sqrt{A_{cr}} = C_2 = \text{Constant}$$

$$= \left(\frac{F}{L^2}\right)L = \frac{\text{Work}}{\text{Area}}$$

$$= \left(\frac{F}{L}\right) = \frac{\text{Force}}{\text{Length}} \tag{3}$$

Note that Moulard [3] presented correlation logarithmic plots of P_s versus A_{cr}. Equation (3) explicitly delineates a plausible P_s and A_{cr} relationship.

Division of Eq. (1) by Eq. (3) yields:

$$\frac{U_{p_{ex}}\ t_{cr}}{\sqrt{A_{cr}}} = \frac{C_1}{C_2} = C_3$$

$$= \text{Dimensionless Constant} \tag{4}$$

The [2] data also confirmed Eq. (4).

Would any of the other available small projectile impact detonation data also substantiate Eqs. (3) and (4)? Analyses of the classic data reported in [6] and [7] (Comp-B and Tetryl), and [8] (TNT), also substantiated Eqs. (3) and (4) to a remarkable degree. The more recent test results for PBX-9404 [1] also corroborated Eqs. (3) and (4) over a rather wide range of projectile diameters. The constants (C_1, C_2, and C_3) are different for the different explosives as shown in Tables 1 through 5, and Figures 3, 4, and 5.

Tables 1-5 list A_{cr} results for Comp-B3, Comp-B, TNT, Tetryl, and PBX-9404, respectively. Figures 3 and 4 illustrate the variation of $P_s\sqrt{A_{cr}}$ as a function of P_s. Figure 5 depicts $U_{p_{ex}}\, t_{cr}/\sqrt{A_{cr}}$ plotted versus P_s. Note that P_s is a function of the impact velocity (V_I) (Appendix A). P_s was employed as a unifying parameter because all of the experimental data were not acquired with a single projectile material (Appendix B). The V_I required to produce a certain P_s will be somewhat different for the different projectile materials (mild steel and copper, or brass).

The values of $P_s\sqrt{A_{cr}}$ and $U_{p_{ex}}\, t_{cr}/\sqrt{A_{cr}}$ for a set of data were, of course, sensitive to the basic input data for the explosive and projectile (Appendices B and C). Some examples which focused attention on this fact are as follows:

The initial computations for the pressed TNT data employed C_o and S values for cast TNT from [12]. When the appropriate C_o and S values for pressed TNT [26] were utilized, the results were much more consistent. Impact velocities, V_I, for the TNT data were difficult to determine precisely from Figure 19 of [8]. However, by making iterative computations with minute changes in V_I, (for a given projectile diameter), very uniform $P_s\sqrt{A_{cr}}$ results were obtained. The minute changes in V_I were in the third and fourth decimal places for V_I expressed in cm/ -sec. This final set of data for TNT (Table 3) also provided very uniform results for the analysis of Section II.B (Table 8), which is independent of A_{cr}.

The density of the [6] Tetryl was $\rho_o = 1.54$ grams/cm^3. However, the density of Tetryl employed to acquire C_1 was 1.655 gram/cm^3 [16]. This result for C_1 was employed since C_1 for $\rho_o = 1.54$ grams/cm^3 was not available. Some of the inconsistency in the Tetryl results may be caused by mismatched C_1 values. The results for PBX-9404 appeared somewhat more consistent when $C_1 = 50.244$ J/cm^2 [4] was employed instead of $C_1 = 64.4$ J/cm^2 from a later source [14].

Although not thoroughly investigated, the projectile shock and particle velocity information (Appendix B) is obviously an important input also. The steel projectiles are assumed to be low carbon mild steels. As such, they may undergo a phase change when shocked above about 130 Kilobars (Kbars). The shock and particle velocity relationship will be different above and below this transition if it existed for the steel of projectiles. Recommendations for further investigation of this possible steel projectile phase transition effect are given in Section IV.

From the above discussion, and that in Appendix C, it should be obvious that obtaining a consistent set of input information for both the explosives and the projectiles was a primary concern of the authors. Some additional methodology concerns are also expressed in the form of action recommendations in Section IV.

Additional relations involving A_{cr} and the shock variables can be derived from Eqs. (1) and (2). For instance, one such relation is:

$$\frac{P_s A_{cr}}{U_{p_{ex}} t_{cr}} = \frac{A_{cr}(\rho_{o_{ex}} U_{s_{ex}})}{t_{cr}} = \frac{\text{Force}}{\text{Length}}$$

$$= \frac{C_2^2}{C_1} = C4 = \text{Constant} \qquad (5)$$

Where

$\rho_{o_{ex}}$ = Initial unshocked density of the explosive

$U_{s_{ex}}$ = Shock front velocity in the explosive

Tables 1 through 5 list $P_s A_{cr}/U_{p_{ex}} t_{cr}$ for the test data considered herein. For certain explosives, the magnitude of this parameter is very uniform. The greatest deviation from uniformity occurs with PBX-9404 for projectile C (19.050). A postulated explanation of the behavior of PBX-9404 for the larger diameter projectiles is given in Section II.B.

It is worth noting that Eq. (3) states that P_s is inversely proportional to $\sqrt{A_{cr}}$. That is:

$$P_s = \frac{C_2}{\sqrt{A_{cr}}} = \frac{C_2}{\sqrt{\pi}} \frac{1}{R_{cr}} \qquad (3)$$

This relation is analogous to a similar expression for the variation of elastic wave stress amplitudes in a slender conical rod [38] or to spherically symmetrical elastic wave amplitudes. In Section II.C, both conical (Eq. (23)) and spherical (Eq. (25)) volume relations are derived from the energy integral (Eq. (20)).

B. Projectile Cross-Section Area (A) Relations

In Appendix F, it was conjectured via analogous reasoning that there was a relation between the critical Ignition Zone Length (IZL) and the projectile cross-section dimensions. This conjecture was verified by empirical numerical experimentation. The resulting expression (Eq. (6F) in Appendix F) is:

$$\frac{IZL}{\sqrt{A}} = \frac{(U_{s_{ex}} - U_{p_{ex}})\, t_{cr}}{\sqrt{A}} = C_5$$

$$= \text{Constant} \qquad (6)$$

C_5 is a constant or practically a constant for a given explosive. $U_{s_{ex}}$, $U_{p_{ex}}$, t_{cr}, and A have all been previously defined in Section II.A.

Table 6 contains the computed values of $IZL/\sqrt{A}$ for each explosive considered herein. These results are graphically depicted in Figures 6 and 7. The average value of $IZL/\sqrt{A}$ for each explosive is considered to be C_5 for that explosive.

Equation (6) states that the IZL is directly proportional to the projectile diameter, or more generally to the square root of the projectile cross-sectional area ($\sqrt{A}$). Note that Eq. (6) is not based on the critical area (A_{cr}) concept.

Regardless of its present uncertain physical interpretation, Eq. (6) must define some natural parameter since its excellent corroboration for the five diverse explosives considered herein can hardly be dismissed as fortuitous or coincidental. One of the better correlations came from the PBX-9404 data over an extremely broad range of conditions. In particular, the correlation was good for the larger projectiles, which exhibited considerable deviation from the norm for the critical area parameters (Section II.A) and energy input parameters (Section II.C).

It is believed that for the larger diameter projectiles, PBX-9404 behaves in the same manner as the propellant LOVA-X1A reported in [41]. It was shown in [41] that ignition (burn) and detonation impact velocities are different at the larger diameters, but are the same at the smaller diameters. Also, the ignition onset always seemed to follow a constant critical energy criteria, but detonation initiation did not do so for the larger diameter projectiles (Figure 3, [41]. See also the discussion in [22], particularly the comments by F. E. Walker with respect to possible low shock pressure effects.

Other empirical relationships can be derived by combining Eq. 6 with Eqs. (1) through (5) of Section II.A. Two of the more plausible results are:

$$\frac{P_s \sqrt{A_{cr} * A}}{(U_{s_{ex}} - U_{P_{ex}})\, t_{cr}} = \frac{P_s \sqrt{A_{cr} * A}}{IZL}$$

$$= C_2/C_5$$

$$= C_6$$

$$= \text{Constant} \qquad (7)$$

$$\frac{\sqrt{A_{cr}}}{\sqrt{A}} * \frac{(U_{s_{ex}} - U_{P_{ex}})}{U_{P_{ex}}} = \frac{\sqrt{A_{cr}}}{\sqrt{A}} \left(\frac{\rho_o}{\rho - \rho_o}\right)_{ex}$$

$$= C_5/C_3$$

$$= C_7$$

$$= \text{Constant} \qquad (8)$$

Results from Eqs. (7) and (8) are tabulated in Table 6 for each data point. They are valid on the boundary between detonation and no-detonation. Note the results for TNT (Table 6) where it is believed that all points are on, or very close, to this boundary.

It was shown via Figures G-1 through G-5 in Appendix G that

$$(P_s - P_{min})\, d_p = \text{Constant} \qquad (9)$$

Where P_{min} is the extrapolated point where $1/d_p$ equals zero, or one-dimensional conditions exist. Since d_p is the projectile diameter, Eq. (9) implies that:

$$(P_s - P_{min}) \sqrt{A} = \text{Constant}$$

$$= C_8 \qquad (10)$$

If Eq. (10) is multiplied by Eq. (6), this yields:

$$(P_s - P_{min})\, (U_{s_{ex}} - U_{P_{ex}})\, t_{cr} = C_5 * C_8$$

$$(P_s - P_{min})\, (IZL) = C_9$$

$$= \text{Constant} \qquad (11)$$

Numerical results, given in Table 7, substantiated Eq. (10) for the five sets of data under investigation (Figures 8 and 9). Equation (11) was valid for pressed TNT, Tetryl and PBX-9404 (Figure 10). Comp-B3 and Comp-B results exhibited a linear variation of $(P_s - P_{min})$ (IZL) as a function of P_s. Thus, for Comp-B3 and Comp-B, C_9 of Eq. (8) is not a constant, but could be written as $C_{10} + C_{11} * P_s$, where C_{10} and C_{11} are constants.

Note that Eqs. (10) and (11) are somewhat analogous to Eqs. (3) and (1), respectively, in Section II.A. In the same manner, there is a similar analogy between Eq. (6) in this section and Eq. (4) in Section II.A. These equations are collected and displayed side by side in Figure 11.

C. Power and Energy Relations

The empirical results of Section II.A, clearly demonstrate the pervasive influence of the critical area over a wide range of conditions for a given explosive. One basic relation (Eq. (3)) and two auxillary relations (Eqs. (4) and (5)) were obtained which were functions of the critical area, the critical time, and the shock variables. These relations were either dimensionless (Eq. (4)) or had the units of energy fluence (Eq. (1)). A basic and persistent question was: How do these relationships fit into overall general relations which govern the physical phenomenia? In other words, what are these general relationships?

Consequently, in search of increased physical insight, additional analysis and empirical numerical exploration with respect to the shock energy and energy input rate was performed as follows:

Consider the projectile as a piston with a transient cross-section area, A(t). A(t) is the variable shock loaded area of the projectile/explosive target interface as described by Moulard ([2], [3], and Appendix D). The total area dependent high shock energy input rate or power input of the piston at this interface is:

$$\frac{dE}{dt} = A(t)\, P_s\, U_{p_{ex}}$$

$$= A(t) \left(\frac{P_s^2}{\rho_o\, U_{s_{ex}}} \right)$$

$$= \dot{E} = J/\mu\text{-sec} \qquad (12)$$

This is the abbreviated form, commensurate with the critical energy fluence criteria as commonly employed (Eq. C-1 of Appendix C). The exact expression commensurate with Eq. C-3 in Appendix C, is:

$$\frac{dE}{dt} = A(t) \left(\frac{\rho_o\, U_s^2\, U_p^2}{U_s - U_p} \right)_{ex}$$

$$= A(t) \frac{P_s^2}{\rho_{o_{ex}} (U_{s_{ex}} - U_{p_{ex}})} \qquad (13)$$

In the following analysis, Eq. (12) will be employed since it is compatible with critical energy flux density ($P_s\ U_{p_{ex}}\ t_{cr} = C_1$) which is utilized extensively.

For simplicity, consider a cylindrical projectile of Radius, R, such that:

$$A(t) = \pi\ r(t)^2$$

$$= \pi\ [R^2 - 2R\ U_{s_p}\ t + (U_{s_p}\ t)^2] \tag{14}$$

Since

$$r(t) = R - U_{s_p}\ t \tag{15}$$

At an arbitrary time, t_1, the energy rate is:

$$\left.\frac{dE}{dt}\right|_{t_1} = A(t_1)\ P_s\ U_{p_{ex}} = (\dot{E})_{t_1} \tag{16}$$

$(\dot{E})_{t_1}$ signifies the time derivative of E, evaluated at t_1. When $t_1 = 0$, then:

$$(\dot{E})_{t_o} = A\ P_s\ U_{p_{ex}} \tag{17}$$

$(\dot{E})_{t_o}$ is the maximum input energy rate. Its numerical values are listed in Table 8 for the five sets of data under investigation.

It is noteworthy that when $t_1 = t_{cr}$, then $(\dot{E})_{t_{cr}}$ can be expressed as follows via the empirical relations established in Section II.A:

$$\left.\frac{dE}{dt}\right|_{t_{cr}} = A_{cr}\ P_s\ U_{p_{ex}}$$

$$= \frac{A_{cr}\ C_1}{t_{cr}}$$

$$= (A_{cr}\ \rho_{o_{ex}}\ U_{s_{ex}})\ U_p{}^2{}_{ex}$$

$$= \frac{A_{cr}\ P_s{}^2}{\rho_{o_{ex}}\ U_{s_{ex}}}$$

$$= \left(\frac{C_2^2}{\rho_{o_{ex}}}\right)\ \left(\frac{1}{U_{s_{ex}}}\right)$$

$$= \frac{\text{Const.}}{U_{s_{ex}}}$$

$$= (\dot{E})_{t_{cr}} \tag{18}$$

Thus, from Eq. [18], $(\dot{E})_{t_{cr}}$ is inversely proportional to the explosive shock velocity; so it is not a constant. However, it should not exhibit order of magnitude variations as delineated below. The importance of the shock velocity influence is indicated by the following postulated upper and lower bounds for $(\dot{E})_{t_{cr}}$.

$$(\dot{E})t_{cr} = \begin{cases} \dfrac{C_2{}^2}{\rho_{o_{ex}} U_{s_f}} & \text{as } t_{cr} \to \infty \\ \dfrac{C_2{}^2}{\rho_{o_{ex}} D_{-ex}} & \text{as } t_{cr} \to 0 \end{cases} \tag{19}$$

Where

U_{s_f} = minimum shock velocity required for self-sustained phonon fission or crystal lattice breakup and disintegration (Appendix G, [46] and [47]).

D_{-ex} = explosive detonation shock velocity (Appendix F, Table F-1).

These estimates for the limits on $(\dot{E})_{t_{cr}}$ are dependent on the assumption that C_2 remains constant at these extreme limits.

Computed values for the shock energy derivative $(\dot{E})_{t_{cr}}$ and its predicted upper and lower bounds (Eq. (19) and Table G-2) are listed in Table 8 and shown versus P_s in Figures 12, 13, and 14 for all five sets of experimental data. $(\dot{E})_{t_{cr}}$ is bounded reasonably well by Eq. (19) with the exception of PBX-9404 at its upper limit. See the comments in Section II.B with respect to PBX-9404 and the large diameter projectiles.

The faired $(\dot{E})_{t_{cr}}$ values for Comp-B3 (Figure 12) and Tetryl (Figure 14) are somewhat speculative because of the scatter in the computed results. More refined computations are planned as described in Section IV.

After observing $(\dot{E})_{t_{cr}}$ versus P_s in Figures 12, 13, and 14, Dr. Joe Foster [42] remarked that the trend was similar to published results for gaseous explosive detonation power versus energy criteria, since P_s is energy per unit volume. Subsequent inquiries revealed [43], [44], and [45] which delineate power and energy requirements for gaseous explosive detonation. The similarity of Figure 6 in [43] for gaseous detonation, and Figures 12, 13, and 14 in this report for solid explosive detonation, illustrates rather vividly the analogous energy and power requirements for both gaseous and solid explosive detonation.

That is, for either solid or gaseous explosives subjected to low shock (or energy) situations, a high energy rate or power input is required to initiate irreversible reactions leading to detonation. Conversely, for both solid and gaseous explosives, high shock pressure (or energy input) require a relatively low power input. In any case, for a given shock pressure loading (or energy input) at least a certain minimum energy input rate (or power) must be applied to either gaseous or solid explosives.

From Eqs. (12) and (14) the total high shock energy (J) may be computed for a cylindrical projectile of radius, R. This is accomplished as follows to find $E(t_1) = E_1$ for an arbitrary time, t_1:

$$E_1 = \int_0^{t_1} A(t)\, P_s\, U_{p_{ex}}\, dt$$

$$= \pi P_s\, U_{p_{ex}} \int_0^{t_1} (R^2 - 2\, R\, U_{s_p}\, t + U_{s_p}{}^2\, t^2)\, dt$$

$$= \frac{\pi}{3} (R^2 + R\, R_1 + R_1{}^2)\, (U_{p_{ex}}\, t_1)\, P_s \qquad (20)$$

Where $R_1 = R - U_{s_p}\, t_1$ (21)

In general, E_1 may be written as:

$$E_1 = \frac{1}{3} (A + \sqrt{A * A_1} + A_1)\, (U_{p_{ex}}\, t_1)\, P_s \qquad (22)$$

Where

A = projectile cross-section area

A_1 = high shock loaded interface area at time t_1 (Appendix D)

Equations 20 and 22 have an interesting interpretation. The quantity:

$$Vol_1 = \frac{1}{3} (A + \sqrt{A \cdot A_1} + A_1)\, (U_{p_{ex}}\, t_1)$$

$$= (A_{v_1})\, (U_{p_{ex}}\, t_1) \qquad (23)$$

is the volume of a general conical frustum whose length is $U_{p_{ex}}\, t_1$ and whose end areas are A and A_1 (Figure 15). A_{v_1} is the volume weighted area of the frustrum cross-section. For a cylindrical projectile:

$$t_1 = (R - R_1)/U_{s_p}$$

where U_{s_p} = shock velocity in the projectile (24)

So that:

$$Vol_1 = \frac{\pi}{3} (R^2 + R * R_1 + R_1{}^2) (R - R_1) \frac{U_{p_{ex}}}{U_{s_p}}$$

$$= \frac{\pi}{3} (R^3 - R_1{}^3) \frac{U_{p_{ex}}}{U_{s_p}} \tag{25}$$

In this form, Vol_1 is one-fourth of the difference between two spherical volumes times the velocity ratio, $U_{p_{ex}}/U_{s_p}$.

The average energy input rate from t = o to t = t_1 is:

$$(\dot{E}_1)_{av} = \frac{E_1}{t_1}$$

$$= A_{v_1} P_s U_{p_{ex}} \tag{26}$$

When $t_1 = 0$, $E_o = 0$ and

$$(\dot{E}_o)_{av} = \left.\frac{dE}{dt}\right|_o = A P_s U_{p_{ex}} \tag{27}$$

If $t_1 = t_{cr}$, then:

$$E_{cr} = \frac{1}{3} (A + \sqrt{A \cdot A_{cr}} + A_{cr}) (U_{p_{ex}} t_{cr}) P_s$$

$$= (A_{v_{cr}}) P_s U_{p_{ex}} t_{cr}$$

$$= (A_{v_{cr}}) C_1$$

$$= (Vol_{cr}) P_s$$

$$= \frac{\pi}{3} (R^3 - R_{cr}{}^3) \frac{P_s U_{p_{ex}}}{U_{s_p}}$$

$$= \frac{\pi}{3} (R^3 - R_{cr}{}^3) \rho_{o_p} U_{p_p} U_{p_{ex}} \tag{28}$$

The average critical energy input rate is:

$$(\dot{E}_{cr})_{av} = \frac{E_{cr}}{t_{cr}} = \frac{(A_{v_{cr}})C_1}{t_{cr}}$$

$$= (A_{v_{cr}}) P_s U_{p_{ex}} \tag{29}$$

If $t_1 = T = R/U_{s_p}$, $r(T) = 0$ and $A_T = 0$. Thus:

$$E_T = \frac{\pi}{3} (R^2) (U_{p_{ex}} T) P_s$$

$$= \frac{A}{3} (U_{p_{ex}} T) P_s$$

$$= A_{v_T} (U_{p_{ex}} T) P_s$$

$$= (Vol_T) P_s$$

$$= \left(\frac{\pi}{3} R^3\right) \left(\frac{P_s U_{p_{ex}}}{U_{s_p}}\right)$$

$$= \left(\frac{\pi}{3} R^3\right) (\rho o_p U_{p_p} U_{p_{ex}}) \qquad (30)$$

This relation has both conical and spherical volume connotations. The average input rate for E_T is:

$$(\dot{E}_T)_{av} = \frac{E_T}{T}$$

$$= \frac{A}{3} P_s U_{p_{ex}} \qquad (31)$$

Table 9 lists computation results for $A_{v_{cr}}$ (Eq. (28)) for the five sets of data being examined. $A_{v_{cr}}$ was employed to compute E_{cr} (via Eq. (28)) and $(\dot{E}_{cr})_{av}$ (via Eq. (29)) and these quantities are given in Table 9. Table 9 also lists numerical results for E_T (via Eq. (30)) and $(\dot{E}_T)_{av}$ (via Eq. (31)).

What is the "appropriate energy input rate?" Is it $A_{cr} P_s U_{p_{ex}}$ or $A_{v_{cr}} P_s U_{p_{ex}}$? The average value, $A_{v_{cr}} P_s U_{p_{ex}}$, for the time interval, t_{cr}, is larger than $A_{cr} P_s U_{p_{ex}}$, and is a more conservative measure of the power input requirements. Certainly $A_{cr} P_s U_{p_{ex}}$ should be considered an absolute bare minimum requirement.

Consider the impact geometry depicted in Figure 16 for typical tests where the areas, A_{oo}, of both the flat plate projectile and explosive target are much greater than A_{cr} for the particular test conditions. Figure 16.A depicts conditions at the instant of contact (t=o).

In Figure 16.B, the time after impact is $t_{cr} = 2W/U_{s_p}$ so the shock in the projectile has reflected back and is at the projectile target interface. Also, at the edges of the projectile/target interface, rarefaction waves have formed, similar to the small projectile impact tests (Figure 1). The high pressure area at the interface is πR_1^2, or A_1 which is much larger than A_{cr} or even $A_{v_{cr}}$ for that particular pressure level. In fact A_1 is approximately equal to A_{oo} and the critical area is greatly exceeded. Thus, the ignition phenomena is essentially area independent. That is, if Eq. (22) is applied to this condition, then:

$$E_{cr} = \frac{1}{3}\left(A_\infty + \sqrt{A_\infty * A_1} + A_1\right) P_s\, U_{p_{ex}}\, t_{cr}$$

$$\approx A_\infty\, P_s\, U_{p_{ex}}\, t_{cr} \qquad (32)$$

Additional tests with large specimen and different plate thickness ($t_{cr} = 2W/U_{s_p}$) yield the familiar constant energy per unit area criteria (for certain explosives, or course).

$$\frac{E_{cr}}{A_\infty} = P_s\, U_{p_{ex}}\, t_{cr}$$

$$= \text{Constant}$$

$$= C_1 \qquad (33)$$

This is area independent and is a special case of the more general area dependent power/energy concept postulated in this section.

III. CONCLUSIONS

This investigation has revealed simple empirical relationships between the cross-section section area (A) and/or the critical cross-section area (A_{cr}) of a small flat faced projectile and certain quantities (P_s, $U_{p_{ex}}$, t_{cr}) which are critical impact shock variables for five different explosives. The uniformity and consistency of the primary empirical relations (Eqs. (3), (4), (6), (10), and (11)) has generated considerable confidence in their validity, although their general physical meaning may not be clear. It is believed that they are portions of overall general relationships, which are physically meaningful. For instance, Eq. (3) ($P_s \sqrt{A_{cr}} = C_2$) was employed to simplify Eq. (18) for $(\dot{E})_{t_{cr}}$ so that the influence of the shock velocity was clearly delineated.

The analysis of the area dependent shock energy input rate (or power) strongly suggests that it is a fundamental parameter. For a given shock pressure input, at least a minimum energy rate $(\dot{E})_{t_{cr}}$ must be applied for a length of time equal to t_{cr}. This detonation criterion for solid explosives is analogous to results reported in the literature [43], [44] and [45] concerning gaseous explosive detonation. It is shown also that the area dependent power input criteria, and the constant energy (P_s $U_{p_{ex}}$ t_{cr}) criteria are indistinguishable when true one-dimensional conditions exist ($A \gg A_{cr}$).

One important spin-off which evolved from this investigation has been the application of a crystal lattice fracture/disintegration criteria [46] to the prediction of minimum shock pressure required to detonate an explosive. Some pertinent results are contained herein (Section II.C and Appendix G), but the analysis and concept are being published in a separate report [47]. Certain phenomena observed in shocked inert materials may also be explained via the crystal lattice disintegration criteria.

IV. RECOMMENDATIONS

A considerable amount of computational refinements and numerical experimentation remain to be accomplished.

a. First of all, the influence of a possible polymorphic phase transformation effect in the mild steel projectiles at approximately 130 Kbars shock pressure needs to be investigated. This may require that two different functions for the steel shock-particle velocity relationship be employed (one above 130 Kbars and one below 130 Kbars). There are a number of papers and reports on this effect (not cited herein) which must be consulted. The present analysis employed a shock-particle velocity function which is best at somewhat higher shock pressures than shown for any of the data considered herein (above 200 Kbars). Some of the nonuniformity in the present results for steel impacts may be caused by an incorrect shock-particle velocity relation rather than any critical energy criteria limitations (particularly for the lower shock pressures and larger projectiles). The criterion for this phase change analysis will be a comparison of the uniformity and consistence of results with those presently obtained.

b. Determine if possible, via literature search, etc., the appropriate values or relationships for the rarefaction shock velocity for both the explosive target and projectile materials. For example, [37] contains such a relationship in terms of the shock and particle velocities. This, and other feasible relations or values, should be employed in the following computations:

1. Recompute A_{cr} and associated relations using the rarefaction shock velocity for the projectile material.

2. Recompute A_{cr} and associated relations using the rarefaction shock velocity for the explosive target material.

3. Recompute A_{cr} and associated relations using the compression shock velocity of the explosive target material.

Compare the paragraphs 1, 2, and 3 results with the present results (which used the projectile compression shock velocity) for uniformity and consistency. The object of all this numerical and input experimentation is to conform more closely to actual physical conditions. This should yield more uniform results from Eqs. (3), (4), (6), (10), and (11).

Note that computation of A_{cr} via the rarefaction shock velocity in the projectile is suggested by Moulard [2]. However, employing the shock velocity of the explosive material (2 or 3, above) may be physically more realistic since the explosive also unloads at the projectile interface via a rarefaction wave (Figure 1). Thus, the explosive rarefaction velocity may be more appropriate for computing A_{cr} than the projectile rarefaction shock velocity.

The application of Fitzgerald's crystal lattice fracture criteria [46], to shocked induced explosive detonation, was deemed important enough to warrant documentation in a separate report [47], which contains several suggestions for future work.

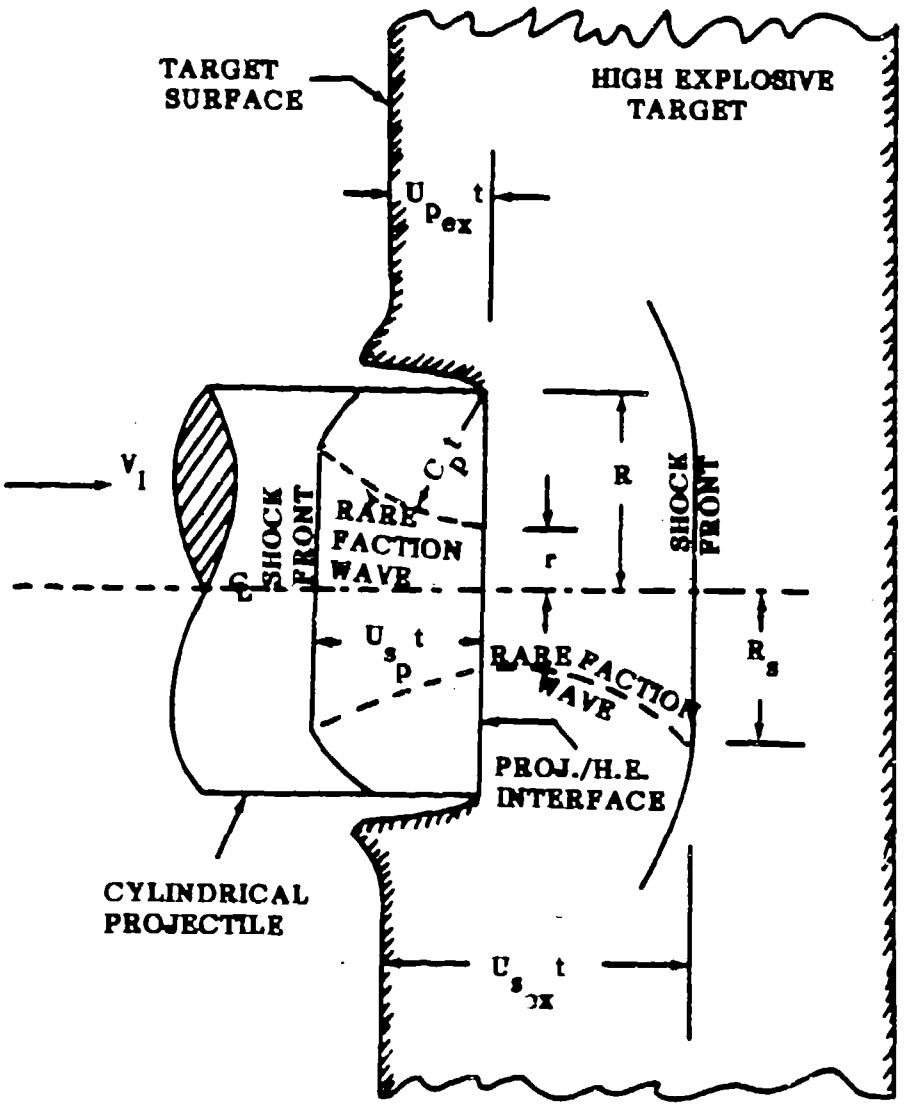

Figure 1. Impact conditions for small flat-faced cylindrical projectiles.

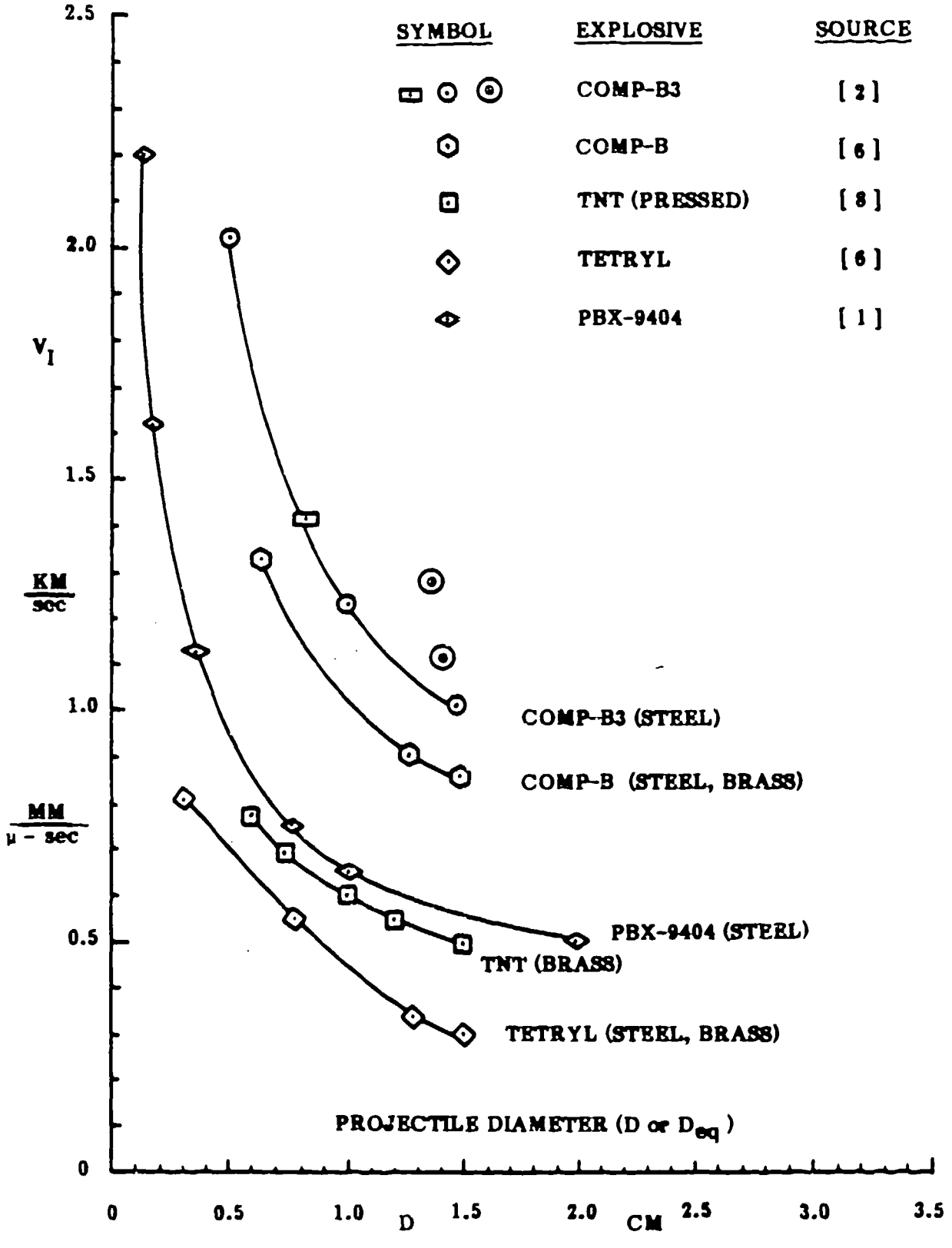

Figure 2. Impact velocity required to initiate detonation in five bare explosives.

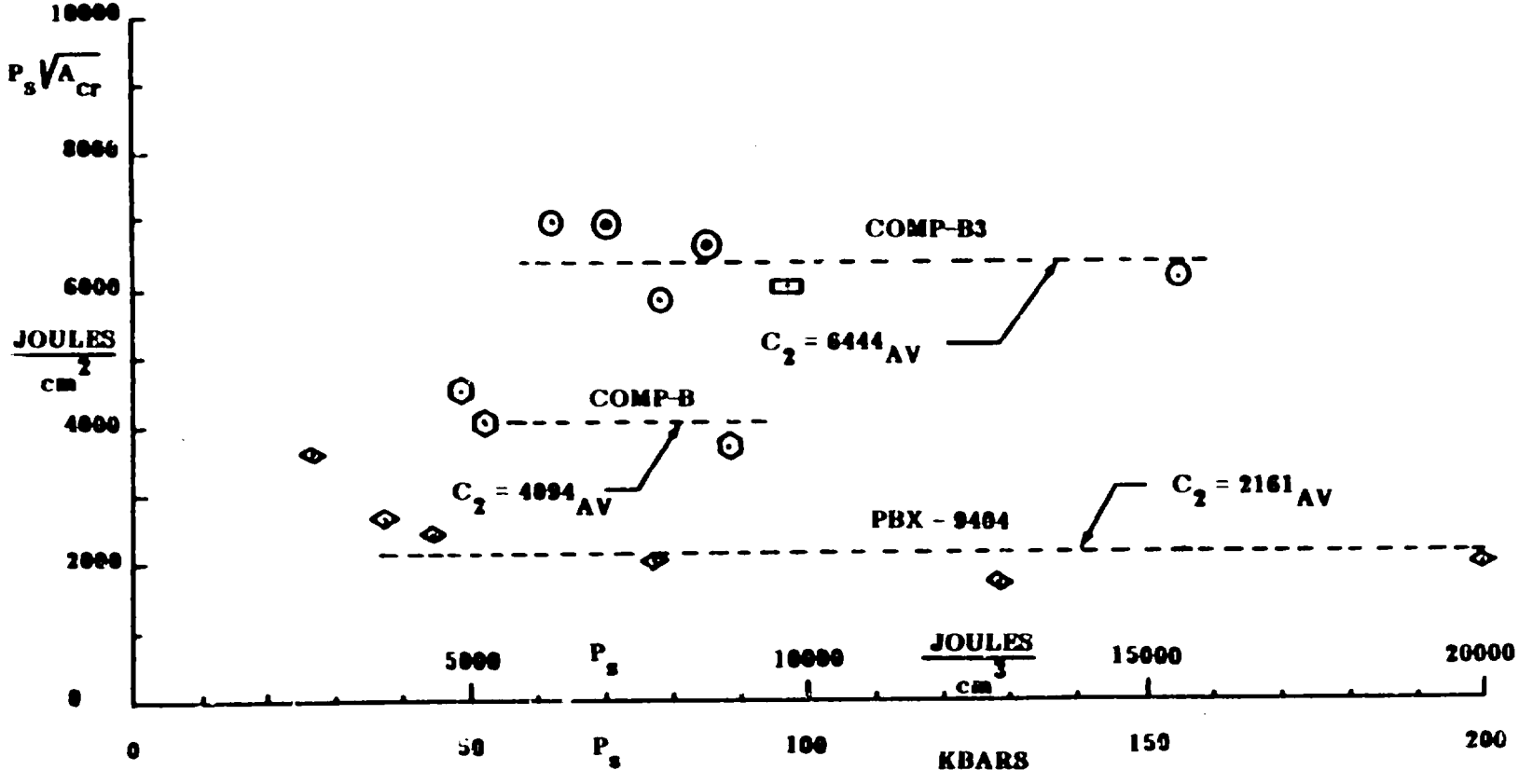

Figure 3. $P_s\sqrt{A_{cr}}$ variation for Comp-B3, Comp-B and PBX-9404.

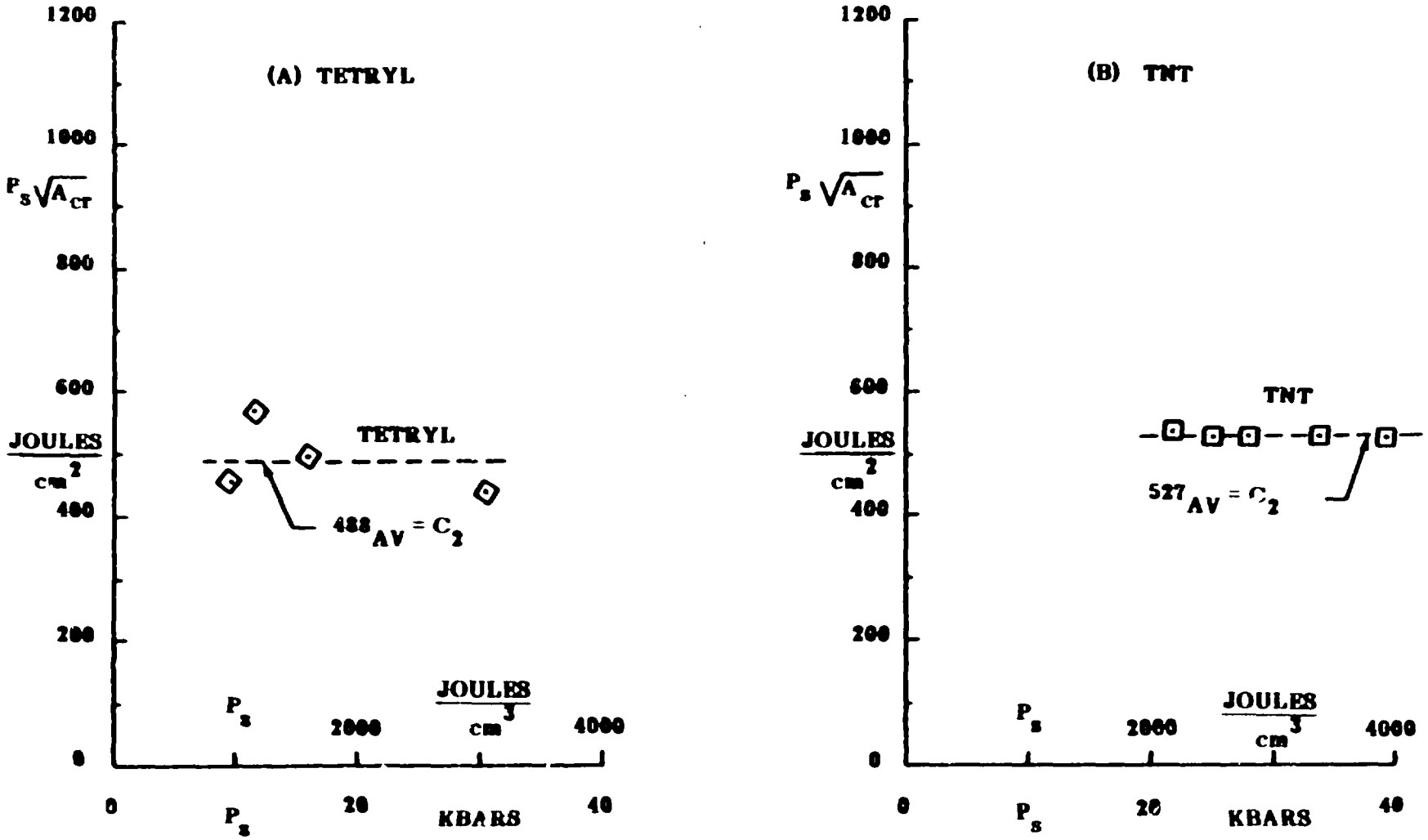

Figure 4. $P_s\sqrt{A_{cr}}$ variation for TNT and Tetryl.

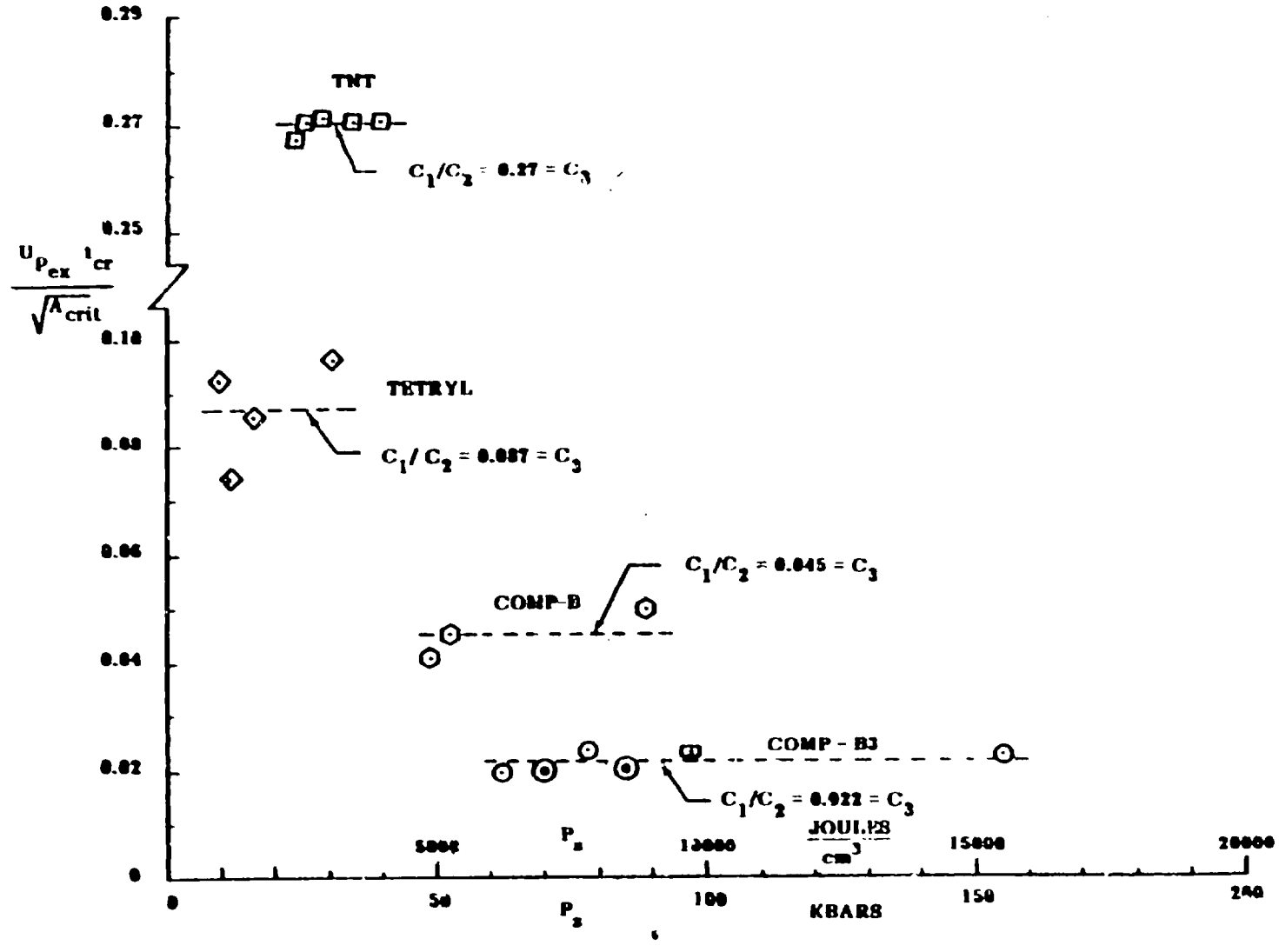

(A) TNT, Comp-B, Tetryl, Comp-B3

Figure 5. $U_{p_{ex}} t_{cr} / \sqrt{A_{cr}}$ variation. (Page 1 of 2 pages.)

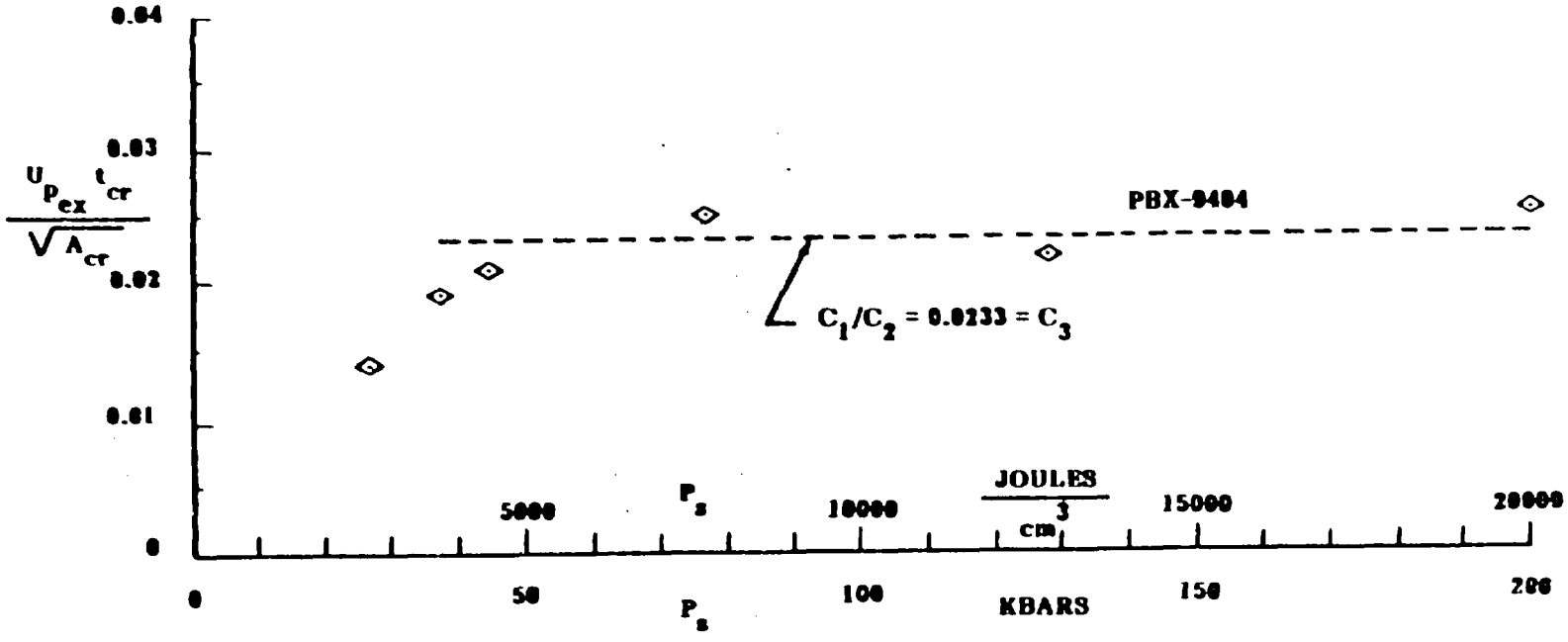

(B) PBX-9494

Figure 5. $U_{p_{ex}} t_{cr} / \sqrt{A_{cr}}$ variation. (Page 2 of 2 pages.)

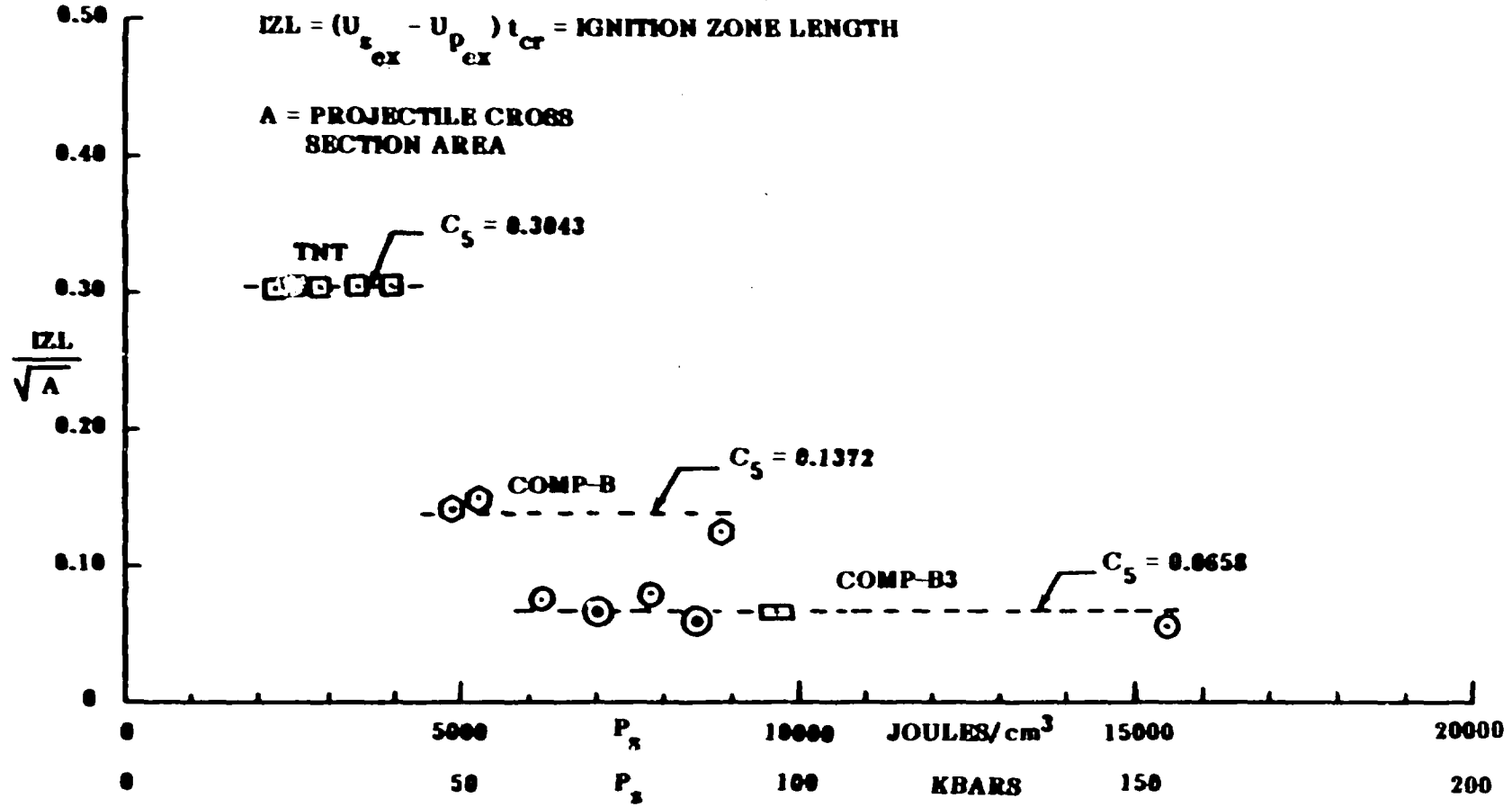

Figure 6. IZL/$\sqrt{A}$ variation for Comp-B3, Comp-B, and TNT.

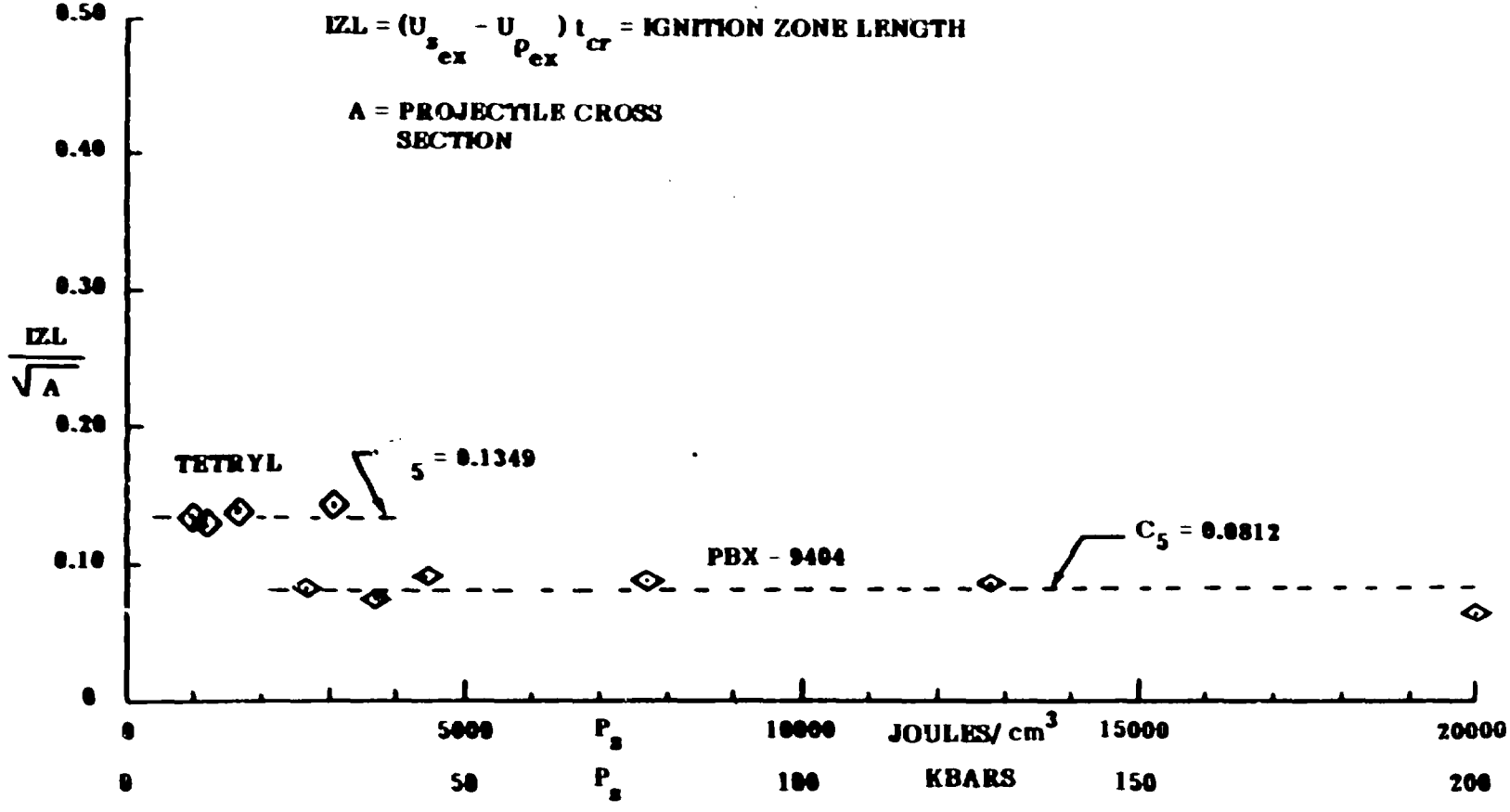

Figure 7. IZL/$\sqrt{A}$ variation for Tetryl and PBX-9404.

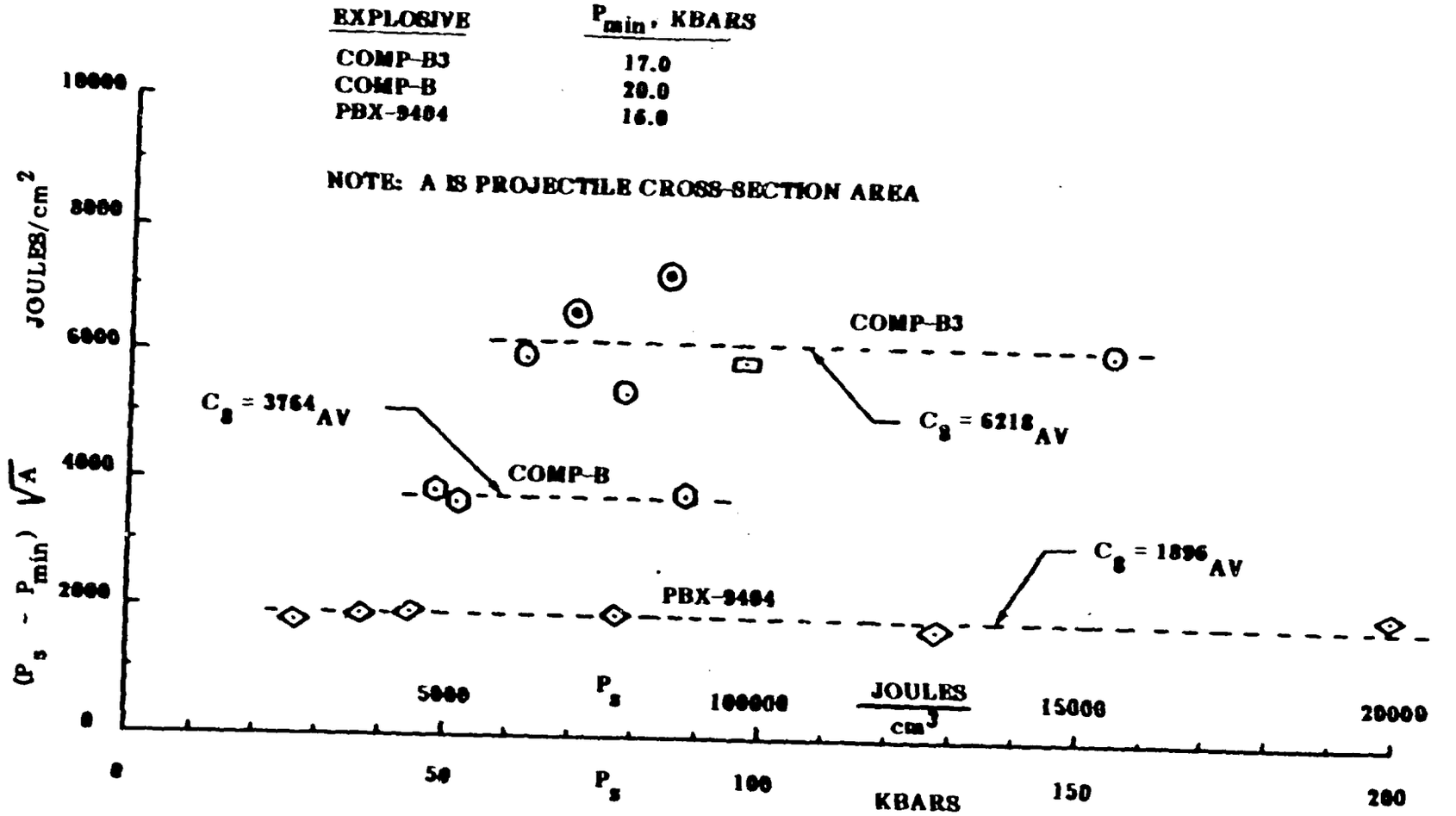

Figure 8. $(P_s - P_{min})\sqrt{A}$ variation for Comp-B3, Comp-B, and PBX-9404.

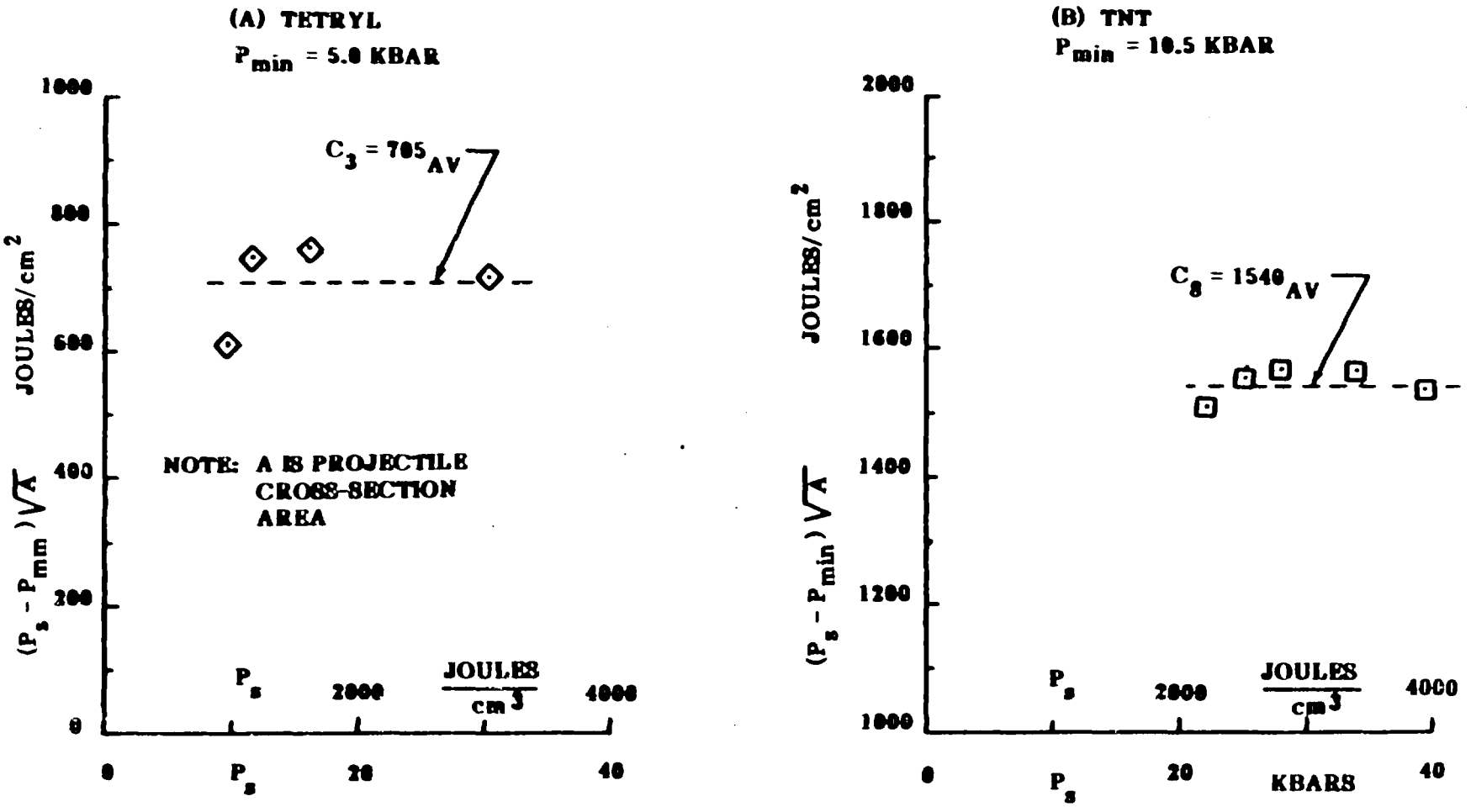

Figure 9. $(P_s - P_{min})\sqrt{A}$ variation for TNT and Tetryl.

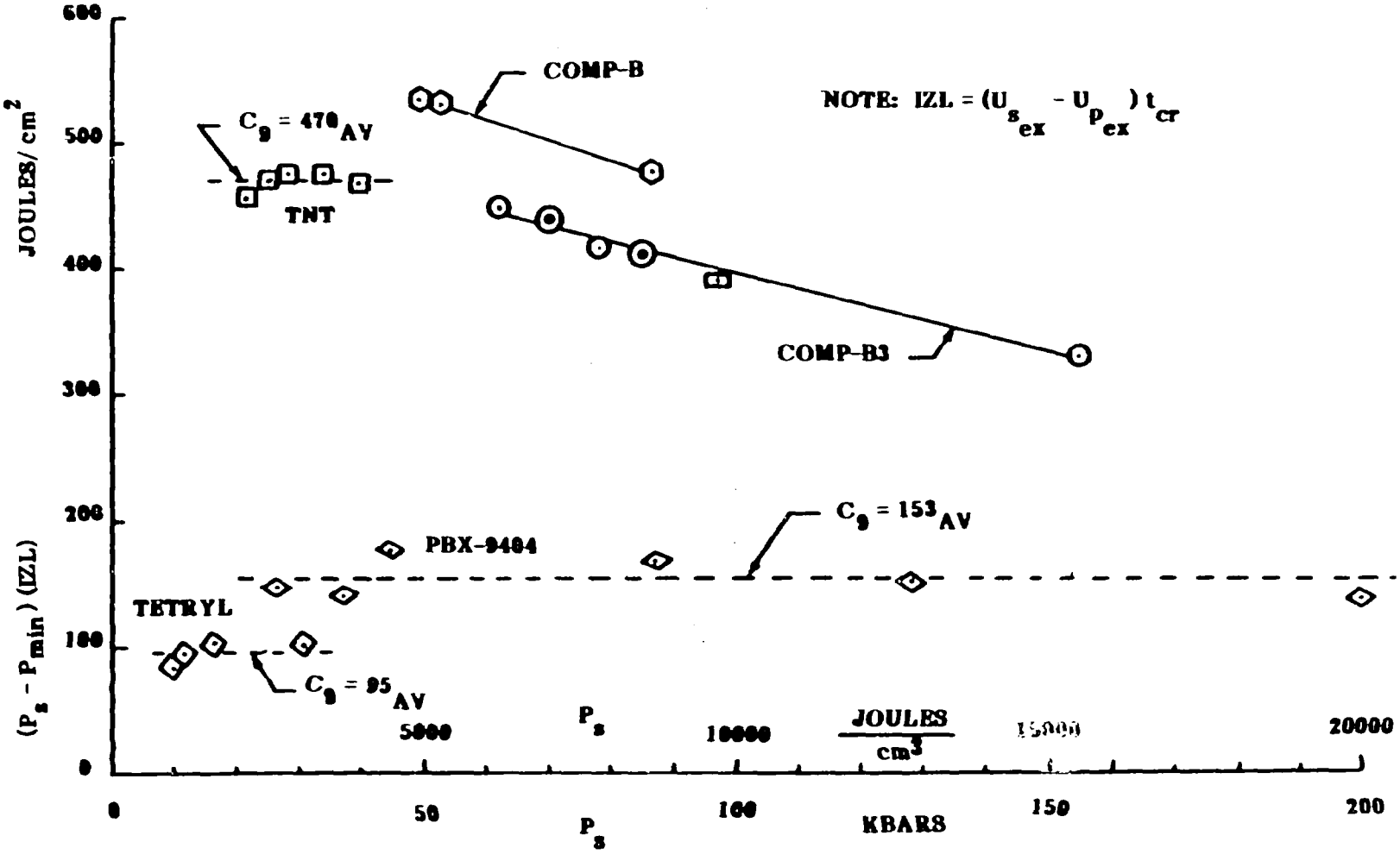

Figure 10. $(P_s - P_{min})$ (IZL) variation for Comp-B3, Comp-B, TNT, Tetryl, and PBX-9404.

EQ. NO.	EQUATION	EQ. NO.	EQUATION
1	$P_s U_{p_{ex}} t_{cr} = C_1$	11	$(P_s - P_{min})(U_{s_{ex}} - U_{p_{ex}})t_{cr} = C_9$
3	$P_s \sqrt{A_{cr}} = C_2$	10	$(P_s - P_{min}) \sqrt{A} = C_8$
4	$\frac{U_{p_{ex}} t_{cr}}{\sqrt{A_{cr}}} = C_3$	6	$\frac{(U_{s_{ex}} - U_{p_{ex}})t_{cr}}{\sqrt{A}} = C_5$

Figure 11. Analogous relations.

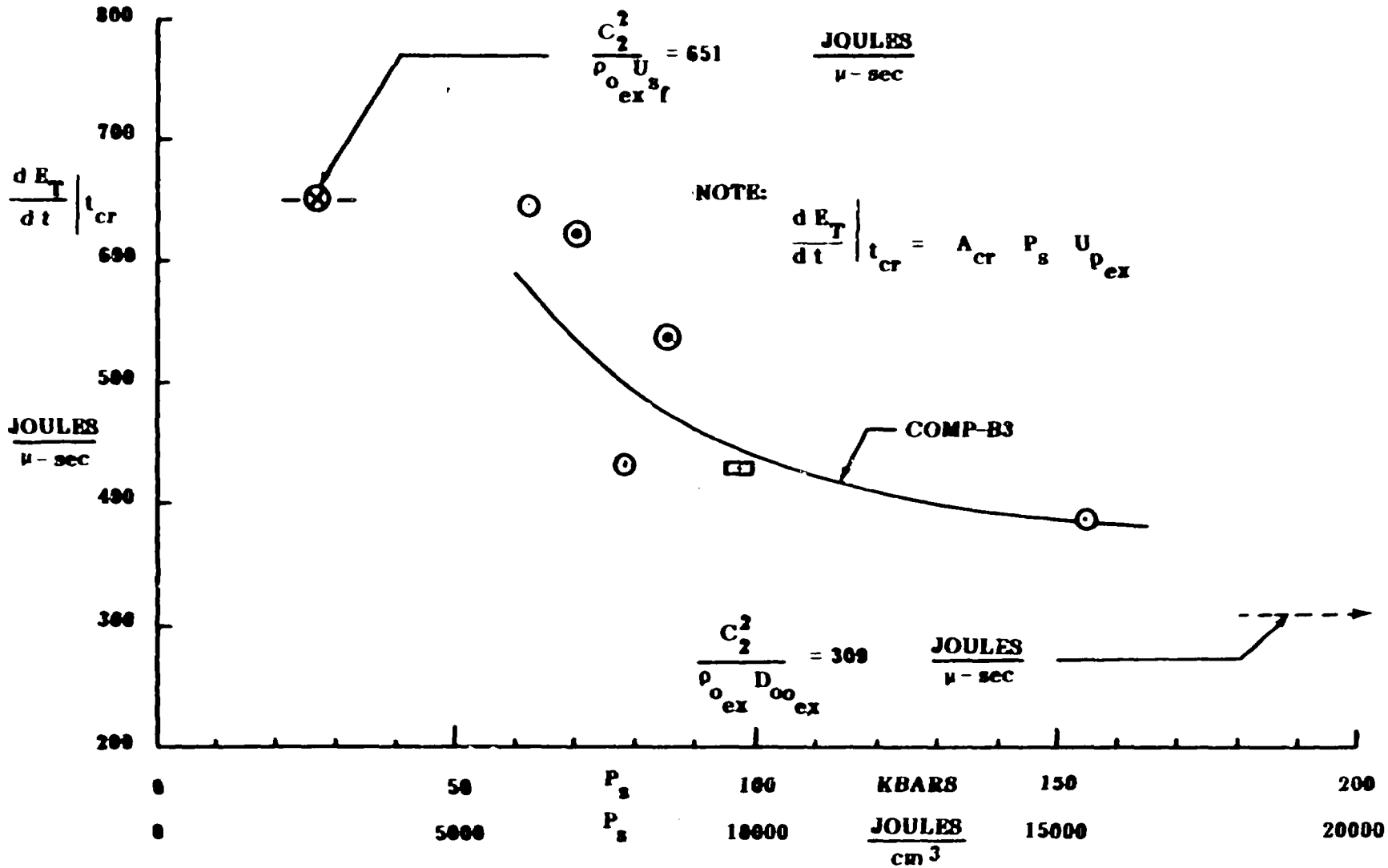

Figure 12. $(\dot{E})_{t_{cr}}$ versus P_s for Comp-B3.

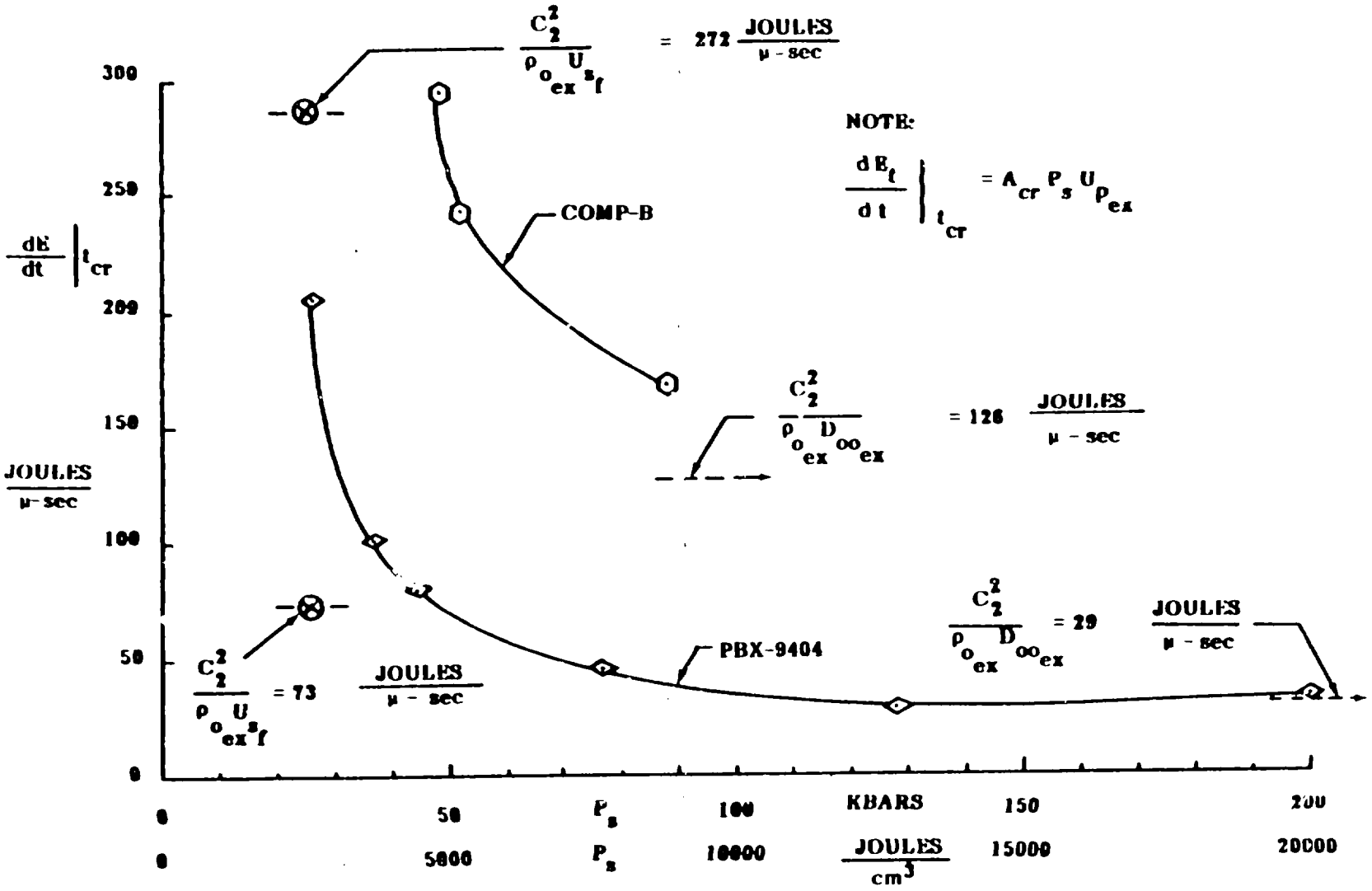

Figure 13. $(\dot{E})_{t_{cr}}$ versus P_s for Comp-B and PBX-9404.

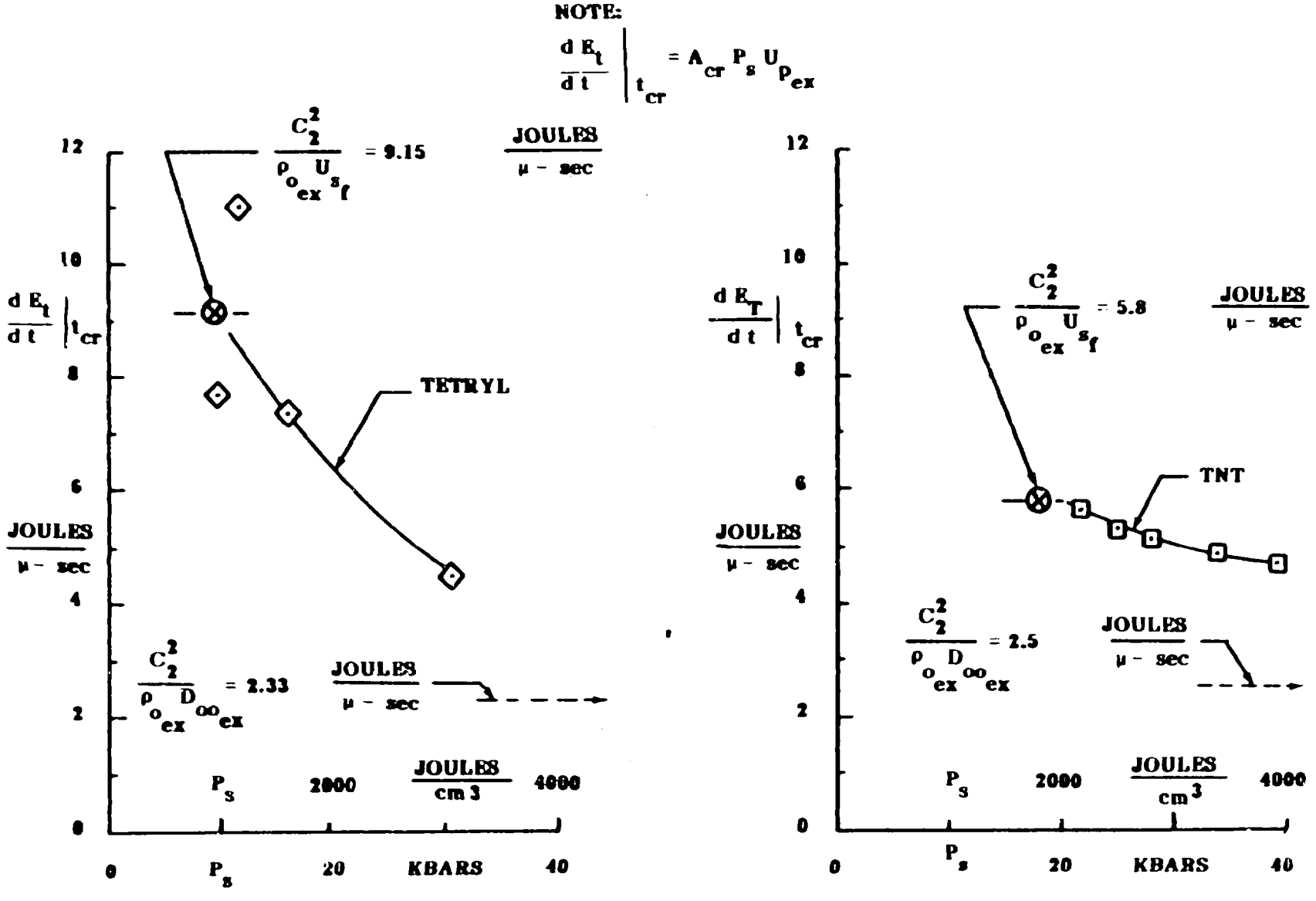

Figure 14. $(\dot{E})_{t_{cr}}$ versus P_s for TNT and Tetryl.

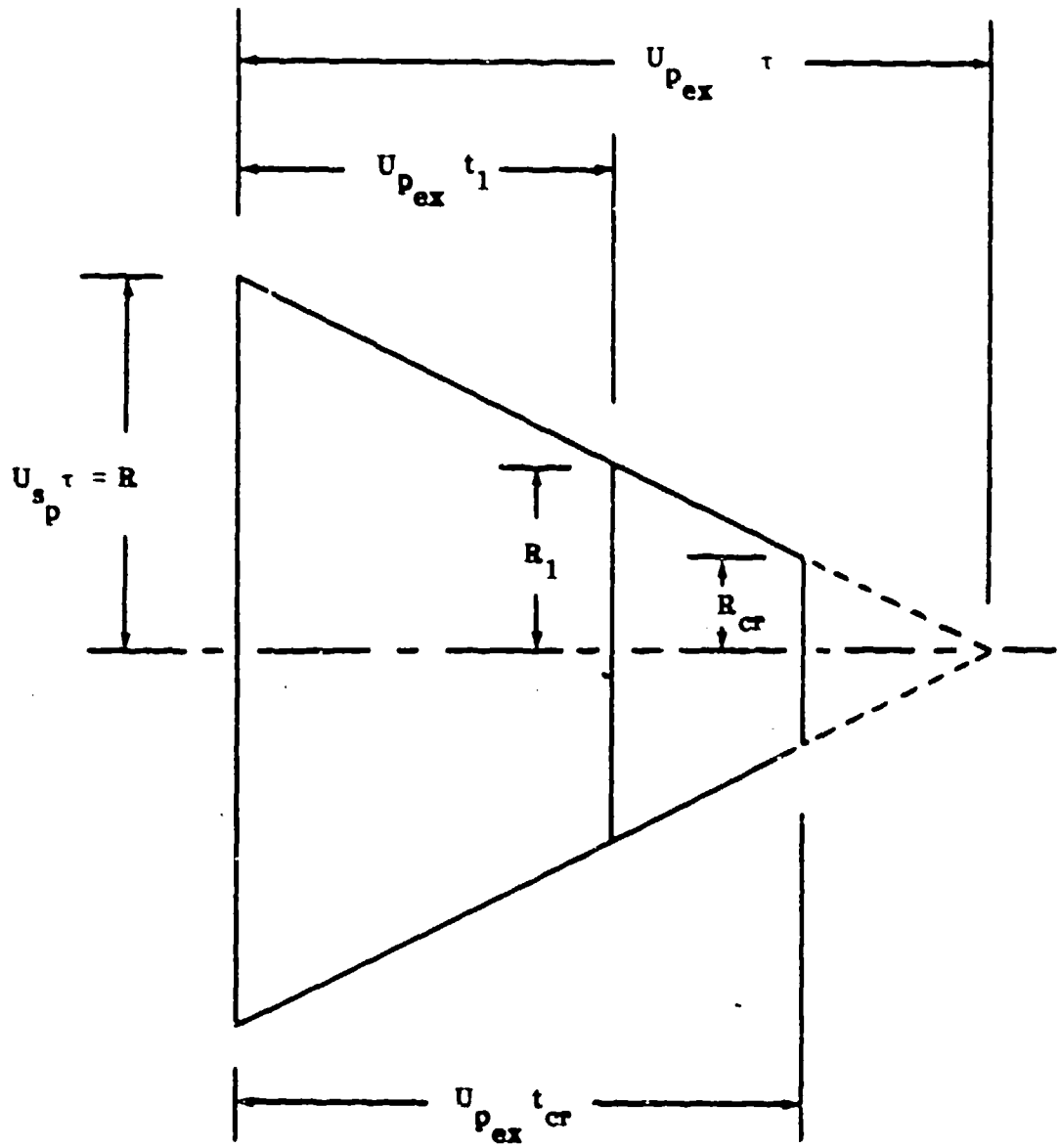

Figure 15. Cone and cone frustum relationships for energy computations. (Sketch not to scale.)

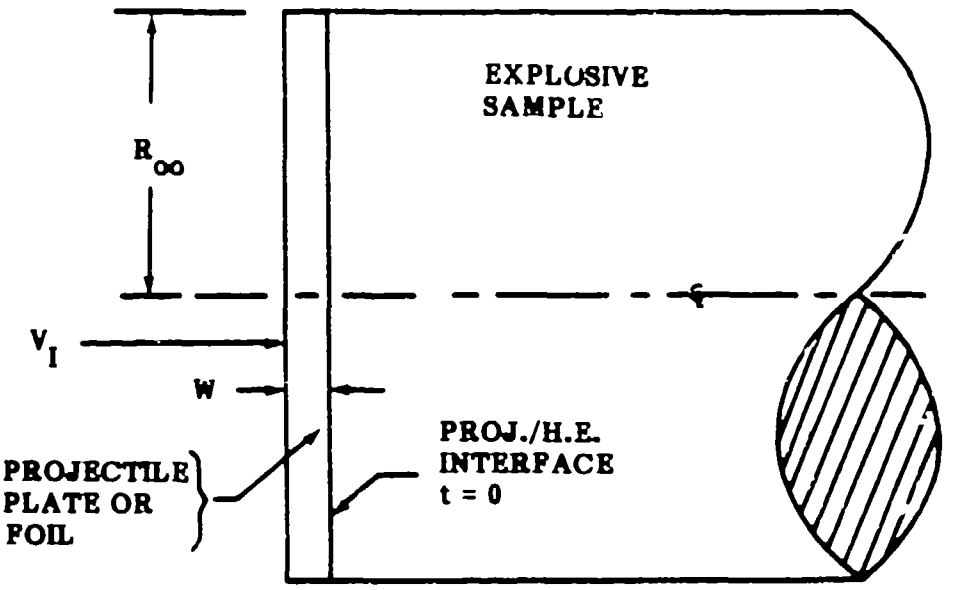

A. t = 0

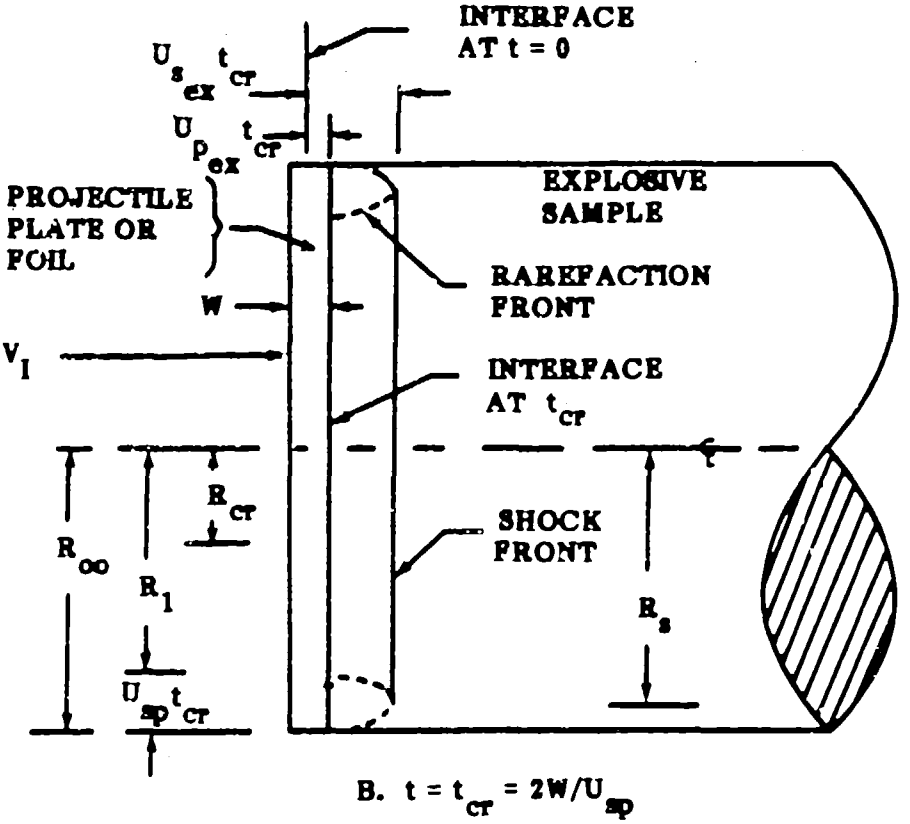

B. $t = t_{cr} = 2W/U_{sp}$

Figure 16. Impact conditions for classic P_s U_{pex} t_{cr} tests.

TABLE 1. Critical Area Computations for Comp-B3.

PROJECTILE	V_I	P_s	U_{p_p}	$U_{p_{ex}}$	$P_s U_{p_{ex}}$	$P_s U_{p_{ex}} t_{cr}$*	t_{cr}	U_{s_p}	$U_{s_p} t_{cr}$**
	$\frac{cm}{\mu-sec}$	$\frac{Joules}{cm^3}$	$\frac{cm}{\mu-sec}$	$\frac{cm}{\mu-sec}$	$\frac{Joules}{cm^2(\mu-sec)}$	$\frac{Joules}{cm^2}$	$\mu-sec$	$\frac{cm}{\mu-sec}$	cm
C(5)	0.2020	15500	0.0440	0.1580	2449.0	140.00	0.0572	0.455	0.0260
R(5X11)	0.1415	9700	0.0275	0.1140	1105.80	140.00	0.1266	0.428	0.0542
A(9X15)	0.1275	8500	0.0250	0.1025	871.25	140.00	0.1607	0.425	0.0683
C(10)	0.1225	7800	0.0240	0.0985	768.30	140.00	0.1822	0.423	0.0771
A(5X15)	0.1105	7000	0.0205	0.0900	630.00	140.00	0.2222	0.417	0.0927
C(15)	0.1000	6200	0.0180	0.0820	508.40	140.00	0.2754	0.413	0.1137

* Value from Table C-1. This is C_1 from Eq. (1).

** $R-R_{cr}$ or $L-L_{cr}$, Eq. (C-4).

TABLE 1. Critical Area Computations for Comp-B3. (Concluded)

PROJECTILE	R_{cr}	A_{cr}	$\sqrt{A_{cr}}$	$P_s\sqrt{A_{cr}}$	$U_{p_{ex}}t_{cr}$	$\frac{U_{p_{ex}}t_{cr}}{\sqrt{A_{cr}}}$	$\frac{C_1}{C_2}$	$\frac{P_s A_{cr}}{U_{p_{ex}} t_{cr}}$	$\frac{C_2^2}{C_1}$
	cm	cm^2	cm	$\frac{Joules}{cm^2}$	cm	~	~	$\frac{Joules}{cm^2}$	$\frac{Joules}{cm^2}$
C(5)	0.2240	0.1576	0.3970	6153.6	0.009034	0.02276	0.02172	270369	296713
R(5X11)(L_1) (W_1)	0.9916 0.3916	0.3883	0.6231	6044.1	0.014432	0.02315	0.02172	260972	296713
A(9X15)(R_1) (r_1)	0.6817 0.5183	0.6160	0.7849	6671.7	0.016472	0.02099	0.02172	317851	296713
C(10)	0.4229	0.5619	0.7496	5846.9	0.017947	0.02394	0.02172	244231	296713
A(5X15)(R_1) (r_1)	0.6573 0.3427	0.9883	0.9941	6958.7	0.019999	0.02012	0.02172	345860	296713
C(15)	0.6363	1.2720	1.1278	$\frac{6992.4}{6444.6_{AV}}$*	0.022583	$\frac{0.02002}{0.02169_{AV}}$**	0.02172	$\frac{349271}{298092_{AV}}$***	296713

* This is C_2, Eq. (3).
** This is $C_3 = C_1/C_2$, Eq. (4).
*** This is $C_4 = C_2^2/C_1$, Eq. (5).

TABLE 2. Critical Area Computations for Comp-B.

PROJECTILE DIAMETER	V_I	P_s	U_{p_p}	$U_{p_{ex}}$	$P_s U_{p_{ex}}$	$P_s U_{p_{ex}} t_{cr}$*	t_{cr}	U_{s_p}	$U_{s_p} t_{cr}$**
cm	$\frac{cm}{\mu\text{-sec}}$	$\frac{Joules}{cm^3}$	$\frac{cm}{\mu\text{-sec}}$	$\frac{cm}{\mu\text{-sec}}$	$\frac{Joules}{cm^2(\mu\text{-sec})}$	$\frac{Joules}{cm^2}$	μ-sec	$\frac{cm}{\mu\text{-sec}}$	cm
0.635	0.1320	8840	0.0230	0.1090	963.56	185.00	0.1920	0.4213	0.0809
1.270	0.0900	5230	0.0162	0.0738	385.97	185.00	0.4793	0.4106	0.1968
1.494	0.0850	4875	0.0152	0.0698	340.28	185.00	0.5437	0.4104	0.2231

* Value from Table C-1. This is C_1 from Eq. (1).
** $R-R_{cr}$ or $L - L_{cr}$, Eq. C-4.

TABLE 2. Critical Area Computations for Comp-B. (Concluded)

PROJECTILE DIAMETER	R_{cr}	A_{cr}	A_{cr}	$P_s\sqrt{A_{cr}}$	$U_{p_{ex}}t_{cr}$	$\frac{U_{p_{ex}}t_{cr}}{\sqrt{A_{cr}}}$	$\frac{C_1}{C_2}$	$\frac{P_s A_{cr}}{U_{p_{ex}} t_{cr}}$	$\frac{C_2^2}{C_1}$
cm	cm	cm^2	cm	$\frac{Joules}{cm^2}$	cm	~	~	$\frac{Joules}{cm^2}$	$\frac{Joules}{cm^2}$
0.635	0.2361	0.1751	0.4185	3699	0.02093	0.05000	0.0452	73980	90597
1.270	0.4382	0.5032	0.7767	4062	0.03537	0.04554	0.0452	89196	90597
1.494	0.5239	0.8622	0.9285	4527	0.03795	0.04087	0.0452	110766	90597
				4095_{AV}*		0.04547_{AV}**		91314_{AV}***	

* This is C_2, Eq. (3).
** This is $C_3 = C_1/C_2$, Eq. (4).
*** This is $C_4 = C_2^2/C_1$, Eq. (5).

TABLE 3. Critical Area Computations for TNT.

PROJECTILE DIAMETER	V_I	P_s	U_{P_p}	$U_{P_{ex}}$	$P_s U_{P_{ex}}$	$P_s U_{P_{ex}} t_{cr}$*	t_{cr}	U_{s_p}	$U_{s_p} t_{cr}$**
cm	$\frac{cm}{\mu\text{-sec}}$	$\frac{Joules}{cm^3}$	$\frac{cm}{\mu\text{-sec}}$	$\frac{cm}{\mu\text{-sec}}$	$\frac{Joules}{cm^2(\mu\text{-sec})}$	$\frac{Joules}{cm^2}$	μ-sec	$\frac{cm}{\mu\text{-sec}}$	cm
0.60	0.0770	3940	0.0107	0.0663	261.04	142.36	0.5454	0.4119	0.2246
0.75	0.0690	3398	0.0093	0.0597	202.83	142.36	0.7019	0.4097	0.2876
1.00	0.0599	2817	0.0078	0.0521	146.87	142.36	0.9693	0.4074	0.3949
1.20	0.0548	2508	0.0069	0.0479	120.05	142.36	1.1859	0.4062	0.4817
1.50	0.0492	2183	0.0061	0.0431	94.16	142.36	1.5118	0.4049	0.6121

* Value from Table C-1. This is C_1 from Eq. (1).
** $R-R_{cr}$ or $L-L_{cr}$, Eq. (C-4).

TABLE 3. Critical Area Computations for TNT. (Concluded)

PROJECTILE DIAMETER	R_{cr}	A_{cr}	$\sqrt{A_{cr}}$	$P_s\sqrt{A_{cr}}$	$U_{p_{ex}}t_{cr}$	$\frac{U_{p_{ex}}t_{cr}}{\sqrt{A_{cr}}}$	$\frac{C_1}{C_2}$	$\frac{P_s A_{cr}}{U_{p_{ex}} t_{cr}}$	$\frac{C_2^2}{C_1}$
cm	cm	cm^2	cm	$\frac{Joules}{cm^2}$	cm	~	~	$\frac{Joules}{cm^2}$	$\frac{Joules}{cm^2}$
0.60	0.0754	0.01785	0.1336	526.4	0.0361	0.2704	02699	1947	1954
0.75	0.0874	0.02401	0.1549	526.5	0.0419	0.2704	02699	1947	1954
1.00	0.1051	0.03469	0.1863	524.7	0.0505	0.2713	02699	1934	1954
1.20	0.1183	0.04398	0.2097	526.0	0.0567	0.2707	02699	1944	1954
1.50	0.1379	0.05976	0.2445	533.5	0.0652	0.2668	02699	1999	1954
				527.4_{AV}*		0.2699_{AV}**		1954_{AV}***	

* This is C_2, Eq. (2).
** This is $C_3 = C_1/C_2$, Eq. (4).
*** This is $C_4 = C_2^2/C_1$, Eq. (5).

TABLE 4. Critical Area Computations for Tetryl.

PROJECTILE DIAMETER	V_I	P_s	U_{p_p}	$U_{p_{ex}}$	$P_s U_{p_{ex}}$	$P_s U_{p_{ex}} t_{cr}$*	t_{cr}	U_{s_p}	$U_{s_p} t_{cr}$**
cm	$\frac{cm}{\mu\text{-sec}}$	$\frac{Joules}{cm^3}$	$\frac{cm}{\mu\text{-sec}}$	$\frac{cm}{\mu\text{-sec}}$	$\frac{Joules}{cm^2(\mu\text{-sec})}$	$\frac{Joules}{cm^2}$	μ-sec	$\frac{cm}{\mu\text{-sec}}$	cm
0.3175	0.0804	3049	0.00840	0.07200	219.58	42.00	0.1913	0.4084	0.0781
0.7620	0.0541	1616	0.00524	0.04886	78.94	42.00	0.5320	0.3933	0.2092
1.2700	0.0433	1159	0.00378	0.03952	45.80	42.00	0.9170	0.3910	0.3585
1.4940	0.0387	960	0.00314	0.03556	34.14	42.00	1.2301	0.3900	0.4797

* Value from Table C-1. This is C_1 from Eq. (1).
** $R-R_{cr}$ or $L-L_{cr}$, Eq. (C-4).

TABLE 4. Critical Area Computations for Tetryl. (Concluded)

PROJECTILE DIAMETER	R_{cr}	A_{cr}	$\sqrt{A_{cr}}$	$P_s\sqrt{A_{cr}}$	$U_{p_{ex}}t_{cr}$	$\frac{U_{p_{ex}}t_{cr}}{\sqrt{A_{cr}}}$	$\frac{C_1}{C_2}$	$\frac{P_s A_{cr}}{U_{p_{ex}} t_{cr}}$	$\frac{C_2^2}{C_1}$
cm	cm	cm^2	cm	$\frac{Joules}{cm^2}$	cm	~	~	$\frac{Joules}{cm^2}$	$\frac{Joules}{cm^2}$
0.3175	0.0806	0.0204	0.1429	435.8	0.0138	0.09637	0.8612	4522	5663
0.7620	0.1718	0.0927	0.3045	491.9	0.0260	0.08538	0.8612	5761	5663
1.2700	0.2765	0.2401	0.4900	568.0	0.0362	0.07395	0.8612	7681	5663
1.4940	0.2673	0.2245	0.4738	454.9	0.0437	0.09232	0.8612	4927	5663
				487.7_{AV}*		0.08700_{AV}**		5723_{AV}***	

* This is C_2, Eq. (3).
** This is $C_3 = C_1/C_2$, Eq. (4).
*** This is C_4, Eq. (5).

TABLE 5. Critical Area Computations for PBX-9404.

PROJECTILE DIAMETER	V_I	P_s	U_{p_p}	$U_{p_{ex}}$	$P_s U_{p_{ex}}$	$P_s U_{p_{ex}} t_{cr}$*	t_{cr}	U_{s_p}	$U_{s_p} t_{cr}$**
cm	$\frac{cm}{\mu\text{-sec}}$	$\frac{Joules}{cm^3}$	$\frac{cm}{\mu\text{-sec}}$	$\frac{cm}{\mu\text{-sec}}$	$\frac{Joules}{cm^2(\mu\text{-sec})}$	$\frac{Joules}{cm^2}$	μ-sec	$\frac{cm}{\mu\text{-sec}}$	cm
0.1270	0.220	20027	0.0543	0.1657	3319.200	50.244	0.01514	0.47074	0.00713
0.1778	0.162	12803	0.0368	0.1251	1602.390	50.244	0.03136	0.42322	0.0132T
0.3556	0.113	7718	0.0233	0.0897	692.094	50.244	0.07260	0.42187	0.03063
0.7620	0.075	4456	0.0140	0.0610	271.999	50.244	0.18472	0.40706	0.07519
1.0160	0.065	3703	0.0117	0.0533	197.335	50.244	0.25461	0.40349	0.10273
1.9050	0.050	2659	0.0085	0.0415	110.305	50.244	0.45550	0.39845	0.18149

* Value from Table C-1. This is C_1 from Eq. (1).
** $R-R_{cr}$ or $L-L_{cr}$, Eq. (C-4).

TABLE 5. Critical Area Computations for PBX-9404. (Concluded)

PROJECTILE DIAMETER	R_{cr}	A_{cr}	$\sqrt{A_{cr}}$	$P_s\sqrt{A_{cr}}$	$U_{p_{ex}}t_{cr}$	$\frac{U_{p_{ex}}t_{cr}}{\sqrt{A_{cr}}}$	$\frac{C_1}{C_2}$	$\frac{P_s A_{cr}}{U_{p_{ex}} t_{cr}}$	$\frac{C_2^2}{C_1}$
cm	cm	cm^2	cm	$\frac{Joules}{cm^2}$	cm	~	~	$\frac{Joules}{cm^2}$	$\frac{Joules}{cm^2}$
0.1270	0.05637	0.00998	0.09992	2001.1	0.00251	0.02511	0.02325	79699	92962
0.1778	0.07563	0.01797	0.13405	1716.2	0.00392	0.02183	0.02325	58621	92962
0.3556	0.14717	0.06805	0.26086	2013.3	0.00651	0.02496	0.02325	80674	92962
0.7620	0.30581	0.29380	0.54203	2415.3	0.01127	0.02079	0.02325	116107	92962
1.0160	0.40527	0.51599	0.71832	2659.9	0.01357	0.01889	0.02325	140814	92962
0.77101	1.9050	1.86753	1.36658	3633.7	0.01890	0.01383	0.02325	262793	92962
				2161.2_{AV}*		0.02232_{AV}**		95183_{AV}***	

* This is C_2, Eq. (3).
** This is $C_3 = C_1/C_2$, Eq. (4).
*** This is $C_4 = C_2^2$, Eq. (5).

Note: The averages for C_2, C_3, and C_4 do not include results for projectile C-1.9050.

TABLE 6. Tabulation of IZL Computations.

EXPLOSIVE	PROJECTILE	$U_{s_{ex}}$	$U_{P_{ex}}$	t_{cr}	IZL	$\sqrt{A}$	$\frac{IZL}{\sqrt{A}}$	$\frac{P_s\sqrt{A \cdot A_{cr}}}{IZL}$	$\frac{IZL}{\sqrt{A}}\frac{\sqrt{A_{cr}}}{U_{P_{ex}}\ t_{cr}}$
		$\frac{cm}{\mu\text{-sec}}$	$\frac{cm}{\mu\text{-sec}}$	μ-sec	cm	cm	~	$\frac{Joules}{cm^2}$	~
COMP-B3	C(5)	0.5760	0.1580	0.0572	0.0239	0.4431	0.0540	113955.6	2.3726
COMP-B3	R(5X11)	0.5000	0.1140	0.1266	0.0489	0.7416	0.0659	91716.2	2.8454
COMP-B3	A(9X15)	0.4800	0.1025	0.1607	0.0607	1.0635	0.0570	117047.4	2.7156
COMP-B3	C(10)	0.4730	0.0985	0.1822	0.0682	0.8862	0.0770	75933.8	3.2164
COMP-B3	A(5X13)	0.4590	0.0900	0.2222	0.0820	1.2534	0.0654	106402.1	3.2505
COMP-B3	C(15)	0.4450	0.0820	0.2754	0.1000	1.3294	0.0752	92984.0	3.7562
							$\overline{0.0658}_{AV}$		
COMP-B	C(6.35)	0.4733	0.1090	0.1920	0.0700	0.5628	0.1243	29758.6	2.4860
COMP-B	C(12.70)	0.4186	0.0738	0.4793	0.1653	1.1255	0.1468	27670.3	3.2235
COMP-B	C(14.94)	0.4120	0.0698	0.5437	0.1861	1.3240	0.1406	32197.7	3.4408
							$\overline{0.1372}_{AV}$		
TNT	C(6.0)	0.3637	0.0663	0.5454	0.1622	0.5317	0.3051	1725.3	1.1283
TNT	C(7.5)	0.3483	0.0597	0.7019	0.2026	0.6647	0.3048	1727.4	1.1272
TNT	C(10.0)	0.3305	0.0521	0.9693	0.2699	0.8862	0.3046	1722.6	1.1227
TNT	C(12.0)	0.3205	0.0479	1.1859	0.3233	1.0635	0.3040	1730.3	1.1230
TNT	C(15.0)	0.3094	0.0431	1.5118	0.4026	1.3294	0.3028	1761.9	1.1349
							$\overline{0.3043}_{AV}$		
TETRYL	C(3.175)	0.28228	0.07200	0.1913	0.0402	0.2814	0.1430	3047.6	1.4839
TETRYL	C(7.620)	0.22046	0.04886	0.5320	0.0913	0.6753	0.1352	3638.3	1.5835
TETRYL	C(12.700)	0.19552	0.03952	0.9170	0.1431	1.1255	0.1271	4469.9	1.7187
TETRYL	C(14.940)	0.18002	0.03556	1.2301	0.1777	1.3240	0.1342	3389.7	1.4536
							$\overline{0.1349}_{AV}$		
PBX-9404	C(1.270)	0.6560	0.1657	0.0151	0.0074	0.1126	0.0659	30365.7	2.6245
PBX-9404	C(1.778)	0.5554	0.1251	0.0314	0.0135	0.1576	0.0856	20049.1	3.9212
PBX-9404	C(3.556)	0.4674	0.0897	0.0726	0.0274	0.3151	0.0870	23141.3	3.4856
PBX-9404	C(7.620)	0.3964	0.0610	0.1847	0.0620	0.6753	0.0917	26339.1	4.4108
PBX-9404	C(10.160)	0.3772	0.0533	0.2546	0.0825	0.9004	0.0742	35847.7	3.9280
PBX-9404	C(19.050)	0.3479	0.0415	0.4555	0.1396	1.6883	0.0827	43938.3	5.9798
							$\overline{0.0812}_{AV}$		

TABLE 7. Tabulation of $(P_s - P_{min})\sqrt{A}$ and $(P_s - P_{min})(IZL)$.

PROJECTILE	EXPLOSIVE	P_s	P_{min}	$P_s - P_{min}$	$\sqrt{A}$	$(P_s - P_{min})\sqrt{A}$	$\frac{IZL}{\sqrt{A}}$	$(P_s - P_{min})(IZL)$
		$\frac{Joules}{cm^3}$	$\frac{Joules}{cm^3}$	$\frac{Joules}{cm^3}$	cm	$\frac{Joules}{cm^2}$	~	$\frac{Joules}{cm^2}$
C(5)	COMP-B3	15500	1700	13800	0.4431	6114.78	0.0540	330.20
R(5X11)	COMP-B3	9700	1700	8000	0.7416	5932.80	0.0659	390.97
A(9X15)	COMP-B3	8500	1700	6800	1.0635	7231.80	0.0570	412.21
C(10)	COMP-B3	7800	1700	6100	0.8862	5405.82	0.0770	416.25
A(5X15)	COMP-B3	7000	1700	5300	1.2534	6643.02	0.0654	434.45
C(15)	COMP-B3	6200	1700	4500	1.3294	5982.30	0.0752	449.87
						6218.42_{AV}	0.0658_{AV}	405.66_{AV}
C(6.35)	COMP-B	8840	2000	6840	0.5628	3849.55	0.1243	478.50
C(12.70)	COMP-B	5230	2000	3230	1.1255	3635.37	0.1468	533.67
C(14.94)	COMP-B	4875	2000	2875	1.3240	3806.50	0.1406	535.19
						3763.81_{AV}	0.1372_{AV}	515.79_{AV}
C(6.0)	TNT	3940	1050	2890	0.5317	1536.61	0.3051	468.82
C(7.5)	TNT	3398	1050	2348	0.6647	1560.72	0.3048	475.71
C(10.0)	TNT	2817	1050	1767	0.8862	1565.92	0.3046	476.98
C(12.0)	TNT	2508	1050	1458	1.0635	1550.58	0.3040	471.38
C(15.0)	TNT	2183	1050	1133	1.3294	1506.21	0.3028	456.08
						1540.01_{AV}	0.3043_{AV}	469.79_{AV}
C(3.175)	TETRYL	3049	500	2549	0.2814	717.29	0.1430	102.57
C(7.620)	TETRYL	1616	500	1116	0.6753	753.63	0.1352	101.89
C(12.700)	TETRYL	1159	500	659	1.1255	741.70	0.1271	94.27
C(14.940)	TETRYL	960	500	460	1.3240	609.04	0.1342	80.64
						705.42_{AV}	0.1349_{AV}	94.84_{AV}
C(1.270)	PBX-9404	20027	1600	18427	0.1126	2074.88	0.0659	136.73
C(1.778)	PBX-9404	12803	1600	11203	0.1576	1765.59	0.0856	151.13
C(3.556)	PBX-9404	7718	1600	6118	0.3151	1927.78	0.0870	167.72
C(7.620)	PBX-9404	4456	1600	2856	0.6753	1928.66	0.0917	176.86
C(10.160)	PBX-9404	3703	1600	2103	0.9004	1893.54	0.0742	140.50
C(19.050)	PBX-9404	2659	1600	1059	1.6883	1787.91	0.0827	147.86
						1896.39_{AV}	812_{AV}	153.47_{AV}

TABLE 8. Energy Input Rates for t = 0 and t_{cr}.

EXPLOSIVE	PROJECTILE	$(\dot{E})t_o$	$(\dot{E})t_{cr}$	$\frac{c_2^2}{\rho_o D_\infty}$	$\frac{c_2^2}{\rho_o U_{s_f}}$	$P_s U_{p_{ex}}$
		JOULES/μ-sec	JOULES/μ-sec	JOULES/μ-sec		JOULES/cm^2(μ-sec)
COMP-B3	C(5)	480.79	385.73	309.25		2449.00
COMP-B3	R(5X11)	608.19	427.19			1105.80
COMP-B3	A(9X15)	985.38	536.65			871.25
COMP-B3	C(10)	603.42	431.76			768.30
COMP-B3	A(5X15)	989.73	622.69			630.00
COMP-B3	C(15)	898.50	646.62		651.32	508.40
COMP-B	C(6.35)	305.16	168.72	126.46		963.56
COMP-B	C(12.70)	488.95	232.82			385.97
COMP-B	C(14.94)	596.51	293.37		271.66	340.28
TNT	C(6.0)	73.80	4.66	2.47		261.04
TNT	C(7.5)	89.81	4.86			202.83
TNT	C(10.0)	115.35	5.10			146.87
TNT	C(12.0)	135.78	5.28			120.05
TNT	C(15.0)	166.41	5.63		5.75	94.16
TETRYL	C(3.175)	17.39	4.49	2.33		219.58
TETRYL	C(7.620)	36.00	7.32			78.94
TETRYL	C(12.700)	58.02	11.00			45.80
TETRYL	C(14.940)	59.85	7.66		9.15	34.14
PBX-9404	C(1.270)	42.15	32.50	28.94		3319.20
PBX-9404	C(1.778)	39.74	28.79			1602.39
PBX-9404	C(3.556)	68.72	47.09			692.09
PBX-9404	C(7.620)	124.03	79.92			272.00
PBX-9404	C(10.160)	159.98	101.82			197.34
PBX-9404	C(19.050)	314.42	206.00		73.38	110.31

NOTE: $\frac{c_2^2}{\rho_o D_\infty}$ and $\frac{c_2^2}{\rho_o U_{s_f}}$ are from Appendix G, Table G-2.

TABLE 9. Tabulation of A_{vcr} Computations.

EXPLOSIVE	PROJECTILE	A	A_{cr}	$\sqrt{A \cdot A_{cr}}$	A_{vcr}	$\sqrt{A_{vcr}}$	$P_s \sqrt{A_{vcr}}$
		cm^2	cm^2	cm^2	cm^2	cm	$\frac{Joules}{cm^2}$
COMP-B3	C(5)	0.1963	0.1576	0.1759	0.1766	0.4202	6513
COMP-B3	R(5X11)	0.5500	0.3883	0.4621	0.4668	0.6832	6627
COMP-B3	A(9X15)	1.1310	0.6160	0.8347	0.8606	0.9277	7885
COMP-B3	C(10)	0.7854	0.5619	0.6643	0.6761	0.8223	6414
COMP-B3	A(5X15)	1.5710	0.9883	1.2460	1.2684	1.1262	7883
COMP-B3	C(15)	1.7673	1.2720	1.4993	1.5129	1.2300	7626
COMP-B	C(6.35)	0.3167	0.1751	0.2355	0.2424	0.4923	4352
COMP-B	C(12.70)	1.2668	0.6032	0.7641	0.8780	0.9370	4901
COMP-B	C(14.94)	1.7530	0.8622	1.2294	1.281_	1.1320	5519
TNT	C(6.00)	0.2827	0.01785	0.07104	0.1239	0.3520	1387
TNT	C(7.50)	0.4418	0.02401	0.10299	0.1896	0.4354	1479
TNT	C(10.00)	0.7854	0.03469	0.16506	0.3284	0.5731	1614
TNT	C(12.00)	1.1310	0.04398	0.22303	0.4660	0.6826	1712
TNT	C(15.00)	1.7673	0.05976	0.32498	0.7174	0.8470	1849
TETRYL	C(3.175)	0.0792	0.0204	0.0420	0.0466	0.2157	658
TETRYL	C(7.620)	0.4560	0.0927	0.2055	0.2514	0.5014	810
TETRYL	C(12.700)	1.2668	0.2401	0.5515	0.6861	0.8283	960
TETRYL	C(14.940)	1.7530	0.2245	0.6273	0.8683	0.9318	895
PBX-9404	C(1.270)	0.0127	0.00998	0.01126	0.0113	0.1063	2128
PBX-9404	C(1.778)	0.0248	0.01797	0.02111	0.0213	0.1460	1869
PBX-9404	C(3.556)	0.0993	0.06805	0.08220	0.0832	0.2884	2226
PBX-9404	C(7.620)	0.4560	0.29380	0.36602	0.3719	0.6098	2717
PBX-9404	C(10.160)	0.8107	0.51599	0.64677	0.6578	0.8112	3004
PBX-9404	C(19.050)	2.8504	1.86753	2.30720	2.3417	1.5303	4069

TABLE 10. Energy and Average Energy Rates for t_{cr} and T.

EXPLOSIVE	PROJECTILE	$E_{t_{cr}}/t_{cr}$ / $A_{vcr} P_s U_{Pex}$	t_{cr} / $C_1/P_s U_{Pex}$	E_{tcr} / $A_{vcr} C_1$	E_T/T / $1/3 A P_s U_{Pex}$	T / R/U_{sp}	E_T / $1/3 A P_s U_{Pex} T$	C_1 / $P_s U_{Pex} t_{cr}$
		Joules/μ-sec	μ-sec	Joules	Joules/μ-sec	μ-sec	Joules	Joules/cm²
COMP-B3	C(5)	432.49	0.0572	24.72	160.24	0.5495	88.04	140.00
COMP-B3	R(5X11)	516.19	0.1266	65.35	202.73	0.5841	118.41	140.00
COMP-B3	A(9X15)	749.80	0.1607	120.49	328.46	0.4118	135.25	140.00
COMP-B3	C(10)	519.45	0.1622	94.65	201.14	1.1820	237.75	140.00
COMP-B3	A(5X15)	799.09	0.2222	177.57	329.91	0.5995	197.79	140.00
COMP-B3	C(15)	769.16	0.2754	211.81	299.49	1.8160	543.87	140.00
COMP-B	C(6.35)	233.56	0.1920	44.84	101.72	0.7548	76.78	185.00
COMP-B	C(12.70)	338.89	0.4793	162.43	162.98	1.5465	252.05	185.00
COMP-B	C(14.94)	436.05	0.5437	237.08	198.84	1.8202	361.92	185.00
TNT	C(6.0)	32.34	0.5454	17.64	24.60	0.7283	17.92	142.36
TNT	C(7.5)	38.46	0.7019	26.99	29.87	0.9153	27.34	142.36
TNT	C(10.0)	48.23	0.9693	46.74	38.45	1.2273	47.19	142.36
TNT	C(12.0)	55.94	1.1859	66.34	45.26	1.4771	66.85	142.36
TNT	C(15.0)	67.55	1.5118	102.13	55.47	1.8523	102.75	142.36
TETRYL	C(3.175)	10.23	0.1913	1.96	5.80	0.3887	2.25	42.00
TETRYL	C(7.620)	19.85	0.5320	10.56	12.00	0.9687	11.62	42.00
TETRYL	C(12.700)	31.42	0.9170	28.82	19.34	1.6240	31.41	42.00
TETRYL	C(14.940)	29.64	1.2301	36.47	19.95	1.9154	38.21	42.00
PBX-9404	C(1.270)	37.51	0.0151	0.57	14.05	0.1349	1.90	50.24
PBX-9404	C(1.778)	34.13	0.0314	1.07	13.25	0.2101	2.78	50.24
PBX-9404	C(3.556)	57.58	0.0726	4.18	22.91	0.4215	9.66	50.24
PBX-9404	C(7.620)	101.17	0.1847	18.67	41.34	0.9360	38.69	50.24
PBX-9404	C(10.160)	129.82	0.2546	33.05	53.33	1.2590	67.14	50.24
PBX-9404	C(19.050)	258.30	0.4555	117.66	104.81	2.3905	250.55	50.24

REFERENCES

1. Bahl, K. L., Vantine, H. C., and Weingart, R. C., "The Shock Initiation of Bare and Covered Explosives by Projectile Impact," paper in the proceedings of the Seventh Symposium (International) on Detonation, 16-19 June 1981, proceedings published as NSWC/MP-82-334, pp. 325-335.

2. Moulard, Henry, "Critical Area Concept for Initiation of a Solid High Explosive by the Impact of Small Projectiles." Paper presented at the Seventh International Colloquium on Gas Dynamics of Explosions and Reactive Systems, FRG, August 1979, published in the AIAA Progress in Astronautics and Aeronautics, Vol. 75, Gas Dynamics of Detonations and Explosions, 1981, pp. 296-302.

3. Moulard, Henry, "Critical Conditions for Shock Initiation of Detonation by Small Projectile Impact," paper in the proceedings of the Seventh Symposium (International) on Detonation, 16-19 June 1981, proceedings published as NSWC/MP-82-334, pp. 316-324.

4. Walker, F. E. and Wasley, R. J., "Critical Energy for Shock Initiation of Heterogeneous Explosives," Explosivstoffe, Nr. 1/1969, pp. 9-13.

5. Gittings, E. F., "Initiation of a Solid Explosive by a Short Duration Shock," paper in the proceedings of the Fourth Symposium (International) on Detonation, 12-15 October 1965, published as report ACR-126, pp. 373-380.

6. Slade, D. C. and Dewey, J., "High Order Initiation of Two Military Explosives by Projectile Impact," U.S. Army Ballistic Research Laboratory, Aberdeen Proving Ground, MD, Report No. 1021, July 1957.

7. Weiss, Milton L. and Litchfield, Elton L., "Projectile Impact Initiation of Condensed Explosives," U. S. Department of the Interior, Bureau of Mines, Report of Investigations 6986, 1966. (Contains [6] data.)

8. Eldh, D., Person, B., Ohlin, B., Johansson, C. H., Ljungberg, S., and Sjolin, T., "Shooting Test with Plane Impact Surface for Determining the Sensitivity of Explosives," Explosivstoffe, Nr. 5/1963, pp. 97-103.

9. Roth, J. F., "The Initiation of Explosives Caused by Action Mechanism," paper presented at the Third Symposium on Chemical Problems Connected With the Stability of Explosives, Ystad, Sweden, 28-30 May 1973.

10. Walsh, J. M., Rice, M. H., McQueen, R. G., and Yarger, F. L., "Shock Wave Compression of Twenty-Seven Metals. Equation of State of Metals," Physical Review, Vol. 108, No. 2, 15 October 1957.

11. McQueen, R. G. and Marsh, S. P., "Equation of State of Nineteen Metallic Elements from Shock Wave Measurements to Two Megabars," Journal of Applied Physics, Vol. 31, No. 7, July 1960.

12. Jameson, R. L., Boyle, V. M., and Sultanoff, M., "Determination Of Shock Hugoniots for Several Condensed Phase Explosives," presented at the Fourth Symposium (International) on Detonation, 12-15 October 1965, proceedings published as ACR-126, pp. 241-247.

13. Lindstrom, I. E., "Planar Shock Initiation of Porous Tetryl," Journal of Applied Physics, Vol. 41, Number 1, January 1970, pp. 337-350.

14. Green, L. G., Nidick, Jr., E. J., and Walker, F. E., "Critical Shock Initiation Energy of PBX-9404, A New Approach," Lawrence Livermore Laboratory, University of California, Livermore, CA, Report UCRL-51522, 25 January 1974.

15. Dobratz, B. M., "LLNL Explosives Handbook, Properties of Chemical Explosives and Explosive Simulants," Report UCRL-52997, 16 March 1981. Lawrence Livermore Laboratory, University of California, Livermore, CA, 94550.

16. Walker, F. E., Green, L. G., and Nidick, Jr, E. J., "Critical Energy for Shock Initiation of Tetryl And A-5," Lawrence Livermore Laboratory University of California, Livermore, CA, Report UCID-16469, 14 March 1974.

17. Roslund, L. A., Watt, J. W. and Coleburn, N. L., "Initiation of Warhead Explosives by the Impact of Controlled Fragments I. Normal Impact," NOLTR-73, 124, 15 August 1973, Naval Ordnance Laboratory, White Oak Silver Spring, MD, 20910.

18. Howe, P., Frey, R., Taylor, B., and Boyle, V., "Shock Initiation and the Critical Energy Concept," paper presented at the Sixth Symposium (International) on Detonation, 24-27 August 1976, proceedings published as ONR-ACR-221, pp. 11-14.

19. Titov, V. M., Silvestrov, V. V., Kravtsov, V. V., and Stadnitshenko, I. A., "Investigation of Some Cast TNT Properties at Low Temperatures," IBID, pp. 36-46.

20. Stresau, R. E. and Kennedy, J. E., "Critical Conditions for Shock Initiation of Detonation in Real Systems," IBID, pp. 68-75.

21. Hayes, D. B., "A P^nT Detonation Criterion from Thermal Explosion Theory," IBID, pp. 760-81.

22. "General Discussion on Shock Initiation and P^2/T," 1. Comments by F. E. Walker; 2. Comments by M. Cowperthwaite; 3. Comments by R. Frey and P. Howe, IBID, pp. 82-88.

23. deLongueville, Y., Fauquignon, C., and Moulard, H., "Initiation of Several Condensed Explosives by a Given Duration Shock Wave," IBID, pp. 105-114.

24. Honodel, C.A., Humphrey, J.R., Weingart, R. C., Lee, R. S., and Kramer, P. "Shock Initiation of TATB Formulations," paper presented at the Seventh Symposium (International) on Detonation, 16-19 June 1981, published as NSWC-MP-82-334, pp. 425-434.

25. Khasainov, B. A., Borisov, A. A., Ermolaev, B. S., and Kurotkov, A. I., "Two-Phase Visco-Plastic Model of Shock Initiation of Detonation in High Density Pressed Explosives," IBID, pp. 435-447.

26. Ramsay, J. B. and Popolato, A., "Analysis of Shock Wave and Initiation Data for Solid Explosives," paper presented at the Fourth Symposium (International) on Detonation, 12-15 October 1965, published as ACR-126, pp. 233-238, by the Office of Naval Research, Department of the Navy, Arlington, VA.

27. Kistiakowsky, G. B., "Initiation of Detonation in Explosives," Third Symposium on Combustion and Flame and Explosion Phenomena, published by the Williams and Wilkins Company, Baltimore, MD, 1949, pp. 560-565.

28. Ubbelohde, A. R., "Transition from Deflagration to Detonation: The Physico-Chemical Aspects of Stable Detonation." IBID, pp. 566-571.

29. Pandow, Mary L., Ockert, K. F., and Shuey, H. M., "Studies of the Diameter Dependence of Detonation Velocity in Solid Composite Propellants; I. Attempts to Calculate Reaction Zone Thickness," paper presented at the Fourth Symposium (International) on Detonation, 12-15 October 1965, pp. 96-101.

30. Pandow, Mary L., Ockert, K. F, and Pratt, T. H., "Studies of the Diameter Dependence of Detonation Velocity in Solid Composite Propellants; II. Prediction of Failure Diameter," paper presented at the Fourth Symposium (International) on Detonation, 12-15 October 1965, pp. 102-106.

31. Gordon, W. E., "Detonation Limits in Condensed Explosives," paper presented at the Fourth Symposium (International) on Detonation, 12-15 October 1965, pp. 179-197.

32. Kusakabe, Masao and Fujiwara, Shuzo, "Effects of Liquid Diluents on Detonation Propagation in Nitromethane," paper presented in the Sixth Symposium (International) on Detonation," 24-27 August 1976, pp. 133-142, published as Report ACR-221, by the Office of Naval Research, Department of the Navy, Arlington, VA.

33. Campbell, A. W. and Engelke, Ray, "The Diameter Effect in High-Density Heterogeneous Explosives," paper presented in the Sixth Symposium (International) on Detonation, 24-27 August 1976, pp. 642-652.

34. Hardy, J. R., Karo, A. M. and Walker, F. E. (1979), "The Molecular Dynamics of Shock and Detonation Phenomena In Condensed Matter." Gasdynamics of Detonations and Explosions: AIAA Progress in Astronautics and Aeronautics, (edited by Bowen, Manson, Oppenheim, and Soloukhin), Vol. 75, pp. 209-225, AIAA, New York.

35. Hardy, J. R., Karo, A. M. Walker, F. E., and Cunningham, W. G., (1981), "The Study Of Shocked-Induced Signals And Coherent Effects in Solids by Molecular Dynamics." Gasdynamics of Detonations and Explosions: AIAA Progress in Astronautics and Aeronautics, (edited by Bowen, Manson, Oppenheim, and Soloukhin), Vol. 87, pp. 9-21, AIAA, New York.

36. Cole, Robert H., Underwater Explosions, Dover Publications, Inc., 180 Varick Street, New York, NY, 1965. pp. 20-30, 145, 233-234, First published by Princeton University Press in 1948.

37. Frey, R., Melani, G., Chawla, M., and Trimble, J., "Initiation of Violent Reaction by Projectile Impact." paper presented at the Sixth Symposium (International) on Detonation, 24-27 August 1976. pp. 325-335. Published as ACR-221 by the Office of Naval Research, Department of the Navy, Arlington, VA.

38. Landon, J. W., and Quinney, H., "Experiments with the Hopkinson Pressure Bar," Proceedings of the Royal Society, A, Vol. 103, 1923, pp. 622-643.

39. Green, Leroy, "Shock Initiation of Explosives by the Impact of Small Diameter Projectiles," paper in the Seventh Symposium (International) on Detonation, 16-19 June 1981, pp. 273-277. Published as NSWC-MP-82-334, Naval Surface Weapons Center, White Oak, Silver Spring, MD.

40. Walker, F. M., Karo, A. M., and Hardy, J. R., "Comparison of Molecular Dynamics Calculations with Observed Initiation Phenomena." IBID, pp. 777-788.

41. Andersen, W. H., "Projectile Impact Ignition Characteristics of Propellants," Report 3420-F, prepared by Shock Hydrodynamics Division, Whittaker Corp., 4716 Vineland Avenue, North Hollywood, CA, 91602, for the U.S. Army Research Office, P. O. Box 12211, Research Triangle Park, NC, 27709, May 1980, (AD Number is A085254).

42. Visit and discussion with Dr. Joe Foster (AD/ALJW), Eglin Air Force Base, Florida, 4 February 1988. Subsequent telecon inquiries were made to Professors R. A. Strehlow (University Of Illinois, Urbana, IL) and J. H. Lee (McGill University, Montreal, Canada).

43. Lee, J. H., Knystautas, R., and Guirao, C. M., "Critical Power Density for Direct Initiation of Unconfined Gaseous Detonations," paper in the Fifteenth Symposium (International) on combustion, Toshi Center Hall, Tokyo, Japan, 25-31 August 1974, pp. 53-67 of the papers organized and published by the Combustion Institute, Pittsburgh, PA, 1974.

44. Knystautas, R. and Lee, J. H., "On the Effective Energy For Direct Initiation of Gaseous Detonations," paper in Combustion and Flame, Vol. 27, 1976, pp. 221-228.

45. Abouseif, G. E., and Toong, T. Y., "On Direct Initiation of Gaseous Detonations," paper in Combustion and Flame, Vol. 45, 1982, pp. 39-46.

46. Fitzgerald, E. R., "Particle Waves and Deformations In Crystalline Solids," book published by Interscience Publishers, a Division of John Wiley and Sons, New York, 1966.

47. Billingsley, J. P. and Adams, C. L., "Application of Crystal Lattice Disintegration Criteria to Compute Minimum Shock Induced Reactive Conditions in Solid Explosives and Inert Materials," U.S. Army MICOM Technical Report RD-88-10, Redstone Arsenal, AL 35898, March 1989.

APPENDIX A

RELATIONS BETWEEN SHOCK PRESSURE (P_s), PARTICLE VELOCITY (U_p), SHOCK VELOCITY (U_s), AND PROJECTILE IMPACT VELOCITY (V_I)

Consider the planar impact geometry depicted in Figure A-1 near the center of the projectile. The shock pressure (P_s) is a function of the material density (P_o), shock velocity (U_s), and particle velocity (U_p).

$$P_s - P_o = \rho_o U_s U_p \approx P_s \tag{A-1}$$

Experimental data reveal that the shock velocity is a linear function of the particle velocity for many materials. C_o and S have been determined for many metals, plastics and explosives. (Appendix B.) C_o is generally the bulk modulus elastic wave velocity.

$$U_s = C_o + SU_p \tag{A-2}$$

The projectile-target interface velocity is:

$$V_i = V_I - U_{p_p} = U_{p_t} \tag{A-3}$$

Interface contact requires that the shock pressure in both target and projectile be equal.

$$P_{s_t} = P_{s_p} \tag{A-4}$$

$$P_{s_t} = \rho_{o_t} U_{p_t} (C_t + S_t U_{p_t}) \tag{A-5}$$

$$P_{s_p} = \rho_{o_p} U_{p_p} (C_p + S_p U_{p_p}) \tag{A-6}$$

Equations (A-3), (A-4), (A-5), and (A-6) are solved simultaneously for U_{p_t}.

$$U_{p_t} = \frac{-B + \sqrt{B^2 - 4AC}}{2A} \tag{A-7}$$

$$A = \rho_{o_t} S_t - \rho_{o_p} S_p \tag{A-8}$$

$$B = \rho_{o_t} C_t + 2\rho_{o_p} S_p V_I + P_{o_p} C_p \tag{A-9}$$

$$C = -\rho_{o_p} (S_p V^2_I + C_p V_I) \tag{A-10}$$

If the projectile and target are similar materials, then Eq. (A-7) becomes indeterminant and:

$$U_p = V_I/2 \tag{A-11}$$

Once U_{p_t} is known, U_{s_t} and $P_{s_t} = P_{s_p}$ may be computed from Eqs. (A-2) and (A-5), respectively.

The problem may be solved graphically via plots of P_{s_p} versus U_{p_p} and P_{s_t} versus U_{p_t} as shown in Figure A-2. The graphical solution can be employed even if the shock velocity is not a linear function of the particle velocity. Either V_I or P_s can be given and the graphical procedure will supply the unknowns.

For example, consider the impact of iron (or mild steel) on Comp-B3 if the impact velocity is 2.02 km/sec. From the x-marked points on Figure A-2:

$$U_{p_{ex}} = 1.58 \text{ km/sec}$$

$$U_{p_p} = 0.44 \text{ km/sec}$$

$$P_s = 155 \text{ Kbars}$$

Conversely, if $P_s = 155$ Kbars had been given, the particle and impact velocities could also be determined.

The following dimensional unit relationships proved very useful in the present computations and literature review:

$$P_s = \rho_o U_s U_p = \frac{\text{Gram}}{\text{cm}^3} \quad \frac{\text{cm}}{\mu\text{-sec}} \quad \frac{\text{cm}}{\mu\text{-sec}}$$

$$= \frac{\text{Gram}}{\text{cm } (\mu\text{-sec})^2} = \text{Megabars} \tag{A-12}$$

$$P \text{ (Kbars)} = 10^3 \text{ P(Megabars)}$$

$$= 10 \text{ P(Gigapascals)}$$

$$= 10^{-8} \text{ P(Pascals)}$$

$$= 10^{-2} \text{ P} \left(\frac{\text{J}}{\text{cm}^3}\right) \tag{A-13}$$

$$\text{P} \left(\frac{\text{J}}{\text{cm}^3}\right) = 100 \text{ P(Kbars)} = 10^5 \text{ P(Mbars)} \tag{A-14}$$

$$1 \text{ bar} = 14.504 \text{ lbs/in.}^2 \tag{A-15}$$

$$= 0.98692 \text{ atmospheres}$$

$$\approx 1 \text{ atmosphere}$$

Note that pressure can be expressed in units of energy per unit volume (J/cm^3).

Note also that impact shock pressures can be enormous. In the above example,

$$P_s = 155 \text{ Kbars} = (155)(14504) \text{ PSI}$$

$$= 2{,}248{,}120 \text{ PSI}$$

$$\approx 2.25 \text{ Million PSI}$$

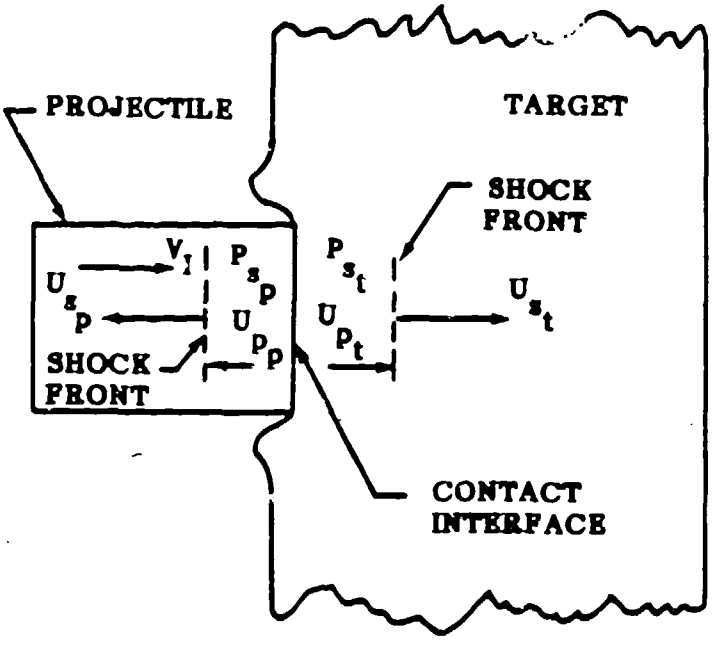

Figure A-1. Initial shock geometry for planar impact.

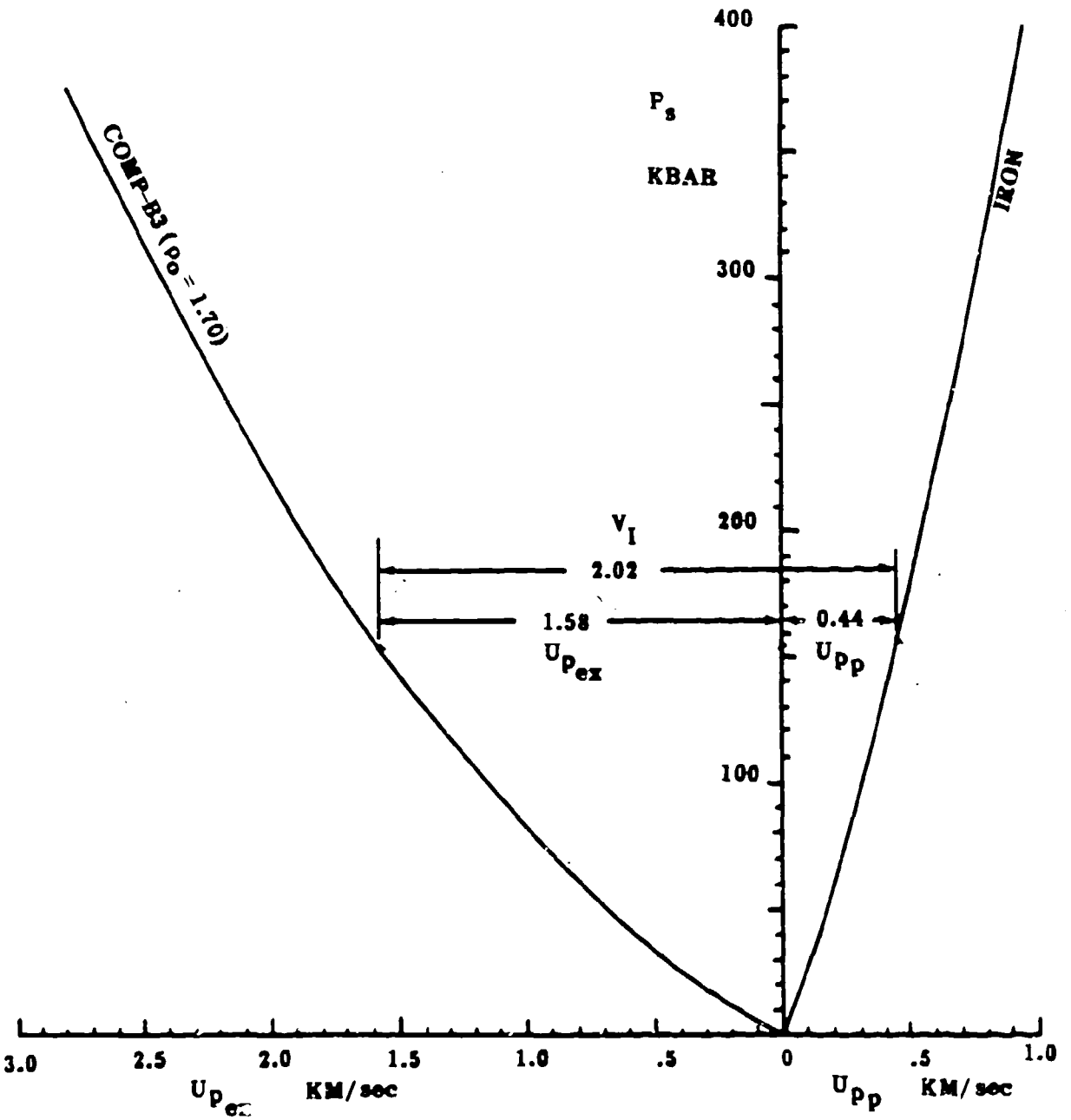

Figure A-2. Shock pressure versus the particle velocity for Comp-B3 and iron.

APPENDIX B

SHOCK COMPRESSION INFORMATION FOR PROJECTILES AND EXPLOSIVES

Moulard [2] employed steel projectiles in his work with Comp-B3. Eldh and coworkers [8] utilized copper projectiles in their experiments with TNT. Slade and Dowey [6] used both brass and steel projectiles to acquire impact detonation data for both Comp-B and Tetryl. The data from [6] is also shown in [7]. Steel projectiles were employed in the impact detonation experiments on PBX 9404 reported in [1].

In our present reexamination of these data, we have used shock loaded iron data for the steel projectiles which were assumed to be mild or low carbon steels. For the brass projectiles, shocked copper data was employed. The shock compression information for copper and iron were obtained from [10] and [11] which are standard sources for such information. The data used are given in Table B-1. See Appendix A for their significance.

Shock compression information for the explosives Comp-B3, Comp-B, TNT, Tetryl, and PBX-9404 is given in Table B-2. The data sources are listed also.

Table B-1. Shocked Projectile Information.

METAL	ρ_o	Co	S	SOURCE
	$\frac{\text{Grams}}{\text{cm}^3}$	$\frac{\text{cm}}{\mu\text{-sec}}$	~	~
Iron	7.840	0.3850	1.580	Refs. 10, 11
Copper	8.903	0.3958	1.497	Refs. 10, 11

Table B-2. Shocked Explosive Information.

EXPLOSIVE	ρ_o	Co	S	SOURCE
	$\frac{\text{Grams}}{\text{cm}^3}$	$\frac{\text{cm}}{\mu\text{-sec}}$	~	~
Comp-B3	1.70	0.303	1.73	Ref. 12
Comp-B	1.70	0.295	1.67*	Ref. 12
TNT (Pressed)	1.635	0.208	2.35	Ref. 26
Tetryl (Porous)	1.50 $\begin{cases} U_s \leq 0.19 \\ U_s \geq 0.19 \end{cases}$	0.020 0.090	4.50 2.67	Ref. 13**
P3X-9404	1.842	0.245	2.48	Refs. 14, 26

*S was modified from 1.58 to 1.67.

**U_s is a nonlinear function of U_p for ρ_o = 1.50 grams/cm^3. Table 2 and Figure 3 of [13] were used to obtain U_s, U_p and P_s. This corresponded closely to the density (1.54) of the tetryl employed in the work reported in [6]. The two linear relations in Table B-2 were employed in the present analysis to represent the nonlinear variation.

APPENDIX C

THE CRITICAL ENERGY CRITERIA AND DATA

As mentioned in the analysis section, the critical energy criteria was developed by the authors of [4] via examination of experimental data reported in [5]. These data were for explosive detonation via thin metallic foil impact (Figure 12). A dependence on the foil thickness (and, hence, shock pulse duration) was noted for these one-dimensional impact conditions. Analysis of these data revealed that:

$$P_s \, U_{p_{ex}} \, t_{cr} = \frac{P^2_s \, t_{cr}}{(\rho_o \, U_s)_{ex}}$$

$$= C_1$$

$$= \text{Energy/Area}$$

$$= \text{Force/Length}$$

$$= \text{Constant} \qquad \text{(C-1)}$$

Where:

P_s = Shock Pressure

$U_{s_{ex}}$ = Shock velocity of the explosive

$U_{p_{ex}}$ = Particle velocity of the explosive behind the shock

$\rho_{o_{ex}}$ = Unshocked density of the explosive

t_{cr} = Constant pressure pulse width, $2W/U_{s_{proj}}$

w = Thickness of metallic foil or plate

$U_{s_{proj}}$ = Shock velocity in metallic foil impactor

C_1 = A constant or practically a constant for many explosives. It has the units of energy per unit area or force per unit length. The magnitude of C_1 is different for different explosives.

Numerous investigators have provided comments on the physical significance of the two forms ($P_s \, I_p \, t$ and $P_s{}^2 t$) of Eq. (C-1). Several papers presented at the Sixth (1976), and Seventh (1981), International Symposiums on Detonation were devoted to this topic. For example, see [18] through [25] and [40].

All explosives do not conform to the critical energy criteria expressed by Eq. (C-1). Roth, in [9], discusses the implications and provides examples for explosives which follow a more general form of Eq. (C-1) which is:

$$P^2_s t_{cr} = f(P_s) \qquad \text{(C-2)}$$

Where $f(P_s)$ is a function of the shock pressure.

In this connection, it should be noted that according to the Cole [36], the form of the energy flux density relation (Eq.(C-1)) omits the contribution of the internal energy ($E-E_o$) and kinetic energy ($U_p^2/2$), and considers only the pressure work (P_s/P). If the internal and kinetic energies are accounted for, then the energy flux density (energy per unit area) is:

$$E_{fd} = \int_o^{t_{cr}} \rho\, U_p \left(E - E_o + \frac{U_p^2}{2} + \frac{P}{\rho}\right) dt$$

$$= \int_o^{t_{cr}} \rho\, U_p\, (U_p\, U_s)\, dt$$

$$= \int_o^{t_{cr}} \left(\frac{\rho_o\, U_p^2\, U_s^2}{U_s - U_p}\right) dt$$

$$= \frac{1}{\rho_o} \int_o^{t_{cr}} \frac{P_s^2\, dt}{\left(U_s - \dfrac{P_s}{\rho_o\, U_s}\right)} \qquad \text{(C-3)}$$

Since in the present case, all quantities to be integrated are constant from $t = o$ to $t = t_{cr}$, then:

$$E_{fd} = \frac{P_s^2\, t_{cr}}{\rho_o \left(U_s - \dfrac{P_s}{\rho_o\, U_s}\right)} = \left(\frac{U_s}{U_s - U_p}\right) P_s\, U_p\, t_{cr}$$

$$= \left(\frac{\rho}{\rho_o}\right) P_s\, U_p\, t_{cr} \qquad \text{(C-4)}$$

Thus:

$$P_s^2\, t_{cr} = \rho_o\, E_{fd} \left(U_s - \frac{P_s}{\rho_o\, U_s}\right) \qquad \text{(C-5)}$$

Which is similar in form to Eq.(C-2) since the RHS of Eq. (C-5) is a function of P_s. The addition of the internal energy and kinetic energy appears important enough to be taken into account in some cases since:

$$\left(\frac{\rho}{\rho_o}\right)_{ex} = \frac{U_{s_{ex}}}{U_{s_{ex}} - U_{p_{ex}}} \qquad \text{(C-6)}$$

Varied from 1.135 to 1.378 for the 5 sets of data considered herein. That is, the internal and kinetic energies contributed from 13 to 37 percent more energy than accounted for by Eq. (C-1).

This would appear to be a subject for further exploration for both the critical energy and critical area concepts, particularly for those explosives which do not comply with Eq. (C-1).

The fact that the detonation energy criteria for many explosives is given by Eq. (C-1) implies that the shock pressure energy (P_s/ρ) is the dominant ignition factor for these explosives, since the internal energy ($E - E_o$) and kinetic energy ($U_p^2/2$) are not included. Andersen [41] agrees with this interpretation since he says:

"Thus the critical energy merely represents the Hugoniot energy delivered during the shock ignition of the material, and has no special relevance to the ignition process other than that a particular pressure is required to cause self-sustained ignition of the material in a particular time."

The authors of [40] provide the following interpretation of P_s/ρ work based on molecular dynamics calculations:

"It appears that what has been called Pdv work is really not a piston action but a summation of the microscopic kinematic processes."

Also, see Cole's comments ([36], pp. 145, 233-234) relative to shock wave energy dissipation in water.

Nominal values for the constant critical energy per unit area (C_1) for Comp-B3, Comp-B, TNT, Tetryl, and PBX 9404 (as employed in the present investigation) are listed in Table C-1. The sources for this information are listed also, along with the density.

As indicated in Tables B-1, B-2, and C-1, the shock compression information necessary to analyze the impact detonation data came from multiple sources. When information from two or more sources (even for the same designated explosive) must be employed, there is still considerable risk of an "apples and oranges" mix. This is because all the factors which affect detonation (composition, manufacturing process, projectile material, grain size, density, etc.) are not necessarily the same in all respects.

For example, Moulard ([3], Figure 2) illustrates differences in the one-dimensional P_s-t sensitivity results for the French and U.S. Comp-B explosives. Apparently, the chemical compositions are slightly different. In the present analysis of Comp-B data [6], a value of $P_s U_{p_{ex}} t_{cr} = 185$ J/cm^2 (Table C-1) was employed. This may not correspond to the U.S. Comp-B, but this value from [15] was all that was available when the impact data were being analyzed.

Moulard ([3], Figure 2) also notes that in [2] "Comp-B3 and Comp-B 1-D sensitivity data were abusively assumed identical." If he is referring to the French Institute of Saint Louis (ISL) Comp-B and Comp-B3, there does not seem to be much difference. We were able to duplicate Moulard's [2] results by using the information listed in this appendix and Appendix B.

Although it could be fortuitous, the information listed in Tables B-1, B-2, and C-1 gave rather consistent and reasonable results when applied to the analysis of the experimental impact detonation data. If more appropriate information becomes available for any of these explosives, the basic impact data will be reexamined to ascertain how well it conforms to the critical area concepts.

TABLE C-1. Explosive Critical Energy.

EXPLOSIVE	ρo_{ex}	$P_s U_{pex} t_{cr}$	$P_s U_{pex} t_{cr}$	SOURCE
	$\frac{Grams}{cm^3}$	$\frac{Joules}{cm^2}$	$\frac{Cal}{cm^2}$	~
Comp-B3	1.73	140.00	33.4	Ref. 2
Comp-B	1.73	185.00	44.2	Ref. 15*
TNT (Pressed)	1.645	142.36	34.0	Ref. 4
TETRYL	1.655	42.00	10.0	Ref. 16
PBX-9404	1.842	50.244	12.00	Ref. 4

*Reported in a revision to [15]. The primary source is [3]. Since one calorie = 4.187 Joules then the energy units conversion factors are:

E(Joules = (4.187) E(Calories)

E(Calories) = (0.2388) E(Joules)

APPENDIX D

MOULARD'S CRITICAL AREA CONCEPT

Moulard's critical area concept is best explained with the aid of Figure 1 which is an adaptation of Figure 2 of [2]. Figure 1 is essentially a more detailed depiction of the shock reflections in the projectile than is shown in Figure A-1 (Appendix A).

Inspection of Figure 1 reveals that at time, t, only a portion of the projectile/explosive interface is still subjected to the original high shock pressure (P_s) generated at impact (t = o). Only that portion of the area enclosed by the radius, r, has been loaded with the initial shock pressure during the time, t. If t is known ($t < R/C_p$), then:

$$r = R - C_p t \tag{D-1}$$

Moulard defines the critical initiation conditions as follows (which is a direct quote from [2]):

"At a given shock pressure, the shock-detonation transition occurs only if a sufficient area of the explosive target is loaded at high pressure for a time equal or greater than the critical shock duration t(p) measured in plane shock-wave experiments at the same shock pressure."

The critical shock duration time, t_{cr}, is known via Eq. (1) if either P_s or V_I is known (see Appendix A).

$$t_{cr} = \frac{C_1}{P_s U_{p_{ex}}} \tag{D-2}$$

The critical area is then:

$$A_{cr} = \pi R^2_{cr} \tag{D-3}$$

Where:

$$R_{cr} = R - C_p\, t_{cr} \tag{D-4}$$

It should be noted that the critical area concept is independent of the constant energy (per unit area) concept. However, t_{cr} must be known from some source as a function of shock pressure or some known variable. For example, see Eq. (C-2) in Appendix C.

In equation D-4, C_p is the velocity of the rarefaction wave from the edge of the projectile. In our data reduction, we employed U_{s_p}, the projectile shock velocity, for C_p.

The above procedure to determine A_{cr} can be adapted for different projectile cross-section shapes. Moulard also cleverly employed rectangular and concentric circular cross-sections to illustrate his point. We were able to verify his calculations of A_{cr} for these shapes (Tables D-1 and D-2). These tables, in conjunction with Table 1 in the main body of this report, illustrate the procedure.

The A_{cr} computations for the tubular or annular projectile [2] are as follows (Figure D-2):

$R - R_1 = U_{s_p} * t_{cr}$

$r_1 - r = U_{s_p} * t_{cr}$

$A_{cr} = \pi(R_1^2 - r_1^2)$ = Area shocked to $P_{s_{cr}}$ level for time, t_{cr}.

The A_{cr} computation for the rectangular bar projectile [2] is as follows (Figure D-3):

$L = U_{s_p} * t_{cr}$

$W = U_{s_p} * t_{cr}$

$L_1 = L - 2\ (\Delta L)$

$W_1 = W - 2\ (\Delta W)$

$A_{cr} = L_1 * W_1$

TABLE D-1. Annular Projectile Critical Area.

ANNULAR PROJECTILE	R	r	R_1	r_1	A_{cr}*	A_{cr}**	A
	cm	cm	cm	cm	cm^2	cm^2	cm^2
A(9x15)	0.75	0.45	0.6817	0.5183	0.6160	0.62	1.131
A(5x15)	0.75	0.25	0.6573	0.3427	0.9883	0.95	1.571

*See Table 1

**Reference 2, Figure 5

TABLE D-2. Rectangular Projectile Critical Area.

RECTANGULAR PROJECTILE	L	W	L_1	W_1	A_{cr}*	A_{cr}**	A
	cm	cm	cm	cm	cm^2	cm^2	cm^2
R(5x11)	1.10	0.50	0.9916	0.3916	0.3883	0.39	0.55

*See Table 1

**Reference 2, Figure 5

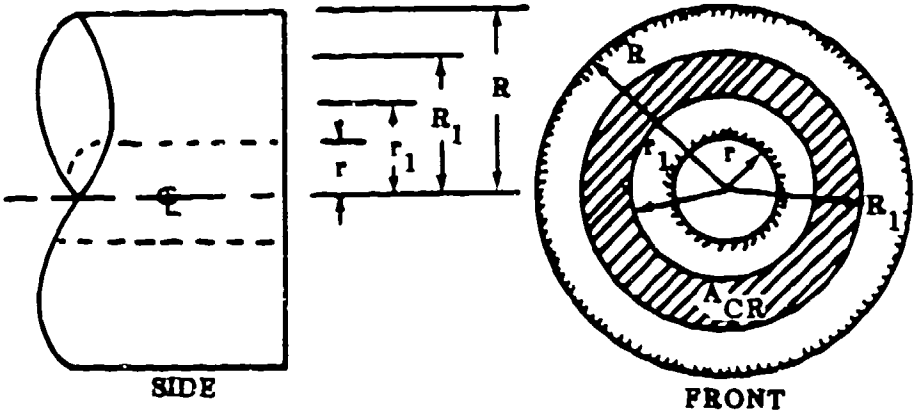

Figure D-1. Critical area geometry for annular projectiles.

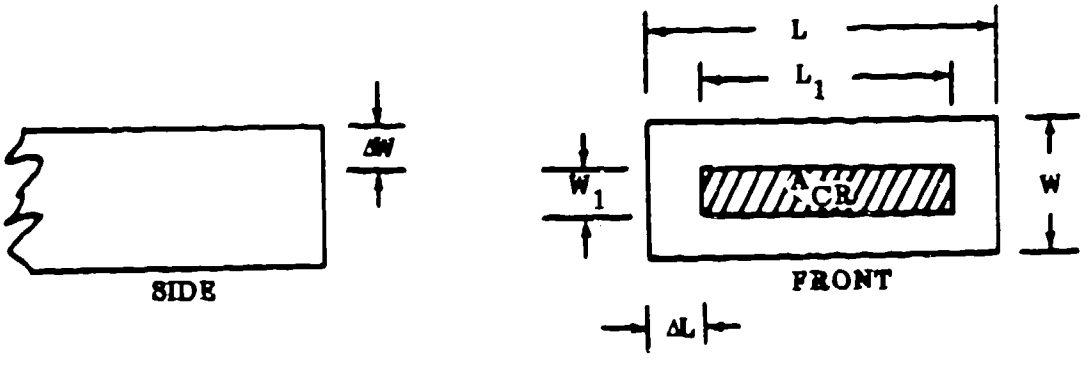

Figure D-2. Critical area geometry for rectangular projectiles.

APPENDIX E

THE JACOBS-ROSLUND EQUATION

An empirical relation, known as the Jacobs equation or the Jacobs-Roslund equation ([1] and [17]) is widely used to predict the critical velocity for projectile induced detonation of an explosive. This equation, in a practical form from [1] is:

$$V_c = \underbrace{\frac{A}{\sqrt{D}}}_{①} \underbrace{(1 + B)}_{②} \underbrace{\left(1 + \frac{CT}{D}\right)}_{③} \qquad \text{(E-1)}$$

Where:

V_c = required fragment impact velocity on warhead case - L/t

A = explosive sensitivity coefficient = $(L)^{3/2}/t$

B = fragment shape coefficient, dimensionless

C = cover place protection coefficient, dimensionless

T = cover plate thickness = L

D = characteristic dimension of the impactor cross-sectional area = L

The significance of the factors ①, ②, and ③ is as follows:

Factor ①

$\frac{A}{\sqrt{D}}$ = V_c for impact detonation of bare explosive with flat faced projectiles.

Factor ②

(1 + B) = Correction factor for projectile shape effects (bare explosive).

Factor ③

$\left(1 + \frac{CT}{D}\right)$ = Correction factor for cased, covered, or protected explosive.

Note that factors (1) and (2) are both concerned with the bare unprotected explosive. The analysis in this report is relevant to factor 1 for planar impact with flat faced projectiles.

For this situation, Eq. (E-1) reduces to:

$$V_c = \frac{A}{\sqrt{D}} \tag{E-2}$$

Or

$$V^2_c D = A^2 = \text{Constant} \tag{E-3}$$

Note that Eqs. (E-2) and (E-3) are equivalent dimensionally to:

$$\frac{\text{Energy}}{\text{Area}} = \rho \frac{L^3 V^2}{L^2} = \rho V^2 L \tag{E-4}$$

and ρ is constant if the projectile material remains unchanged.

Table E-1 and Figure E-1 contain the computed values of A for the explosives considered in the present study. Figure E-1 reveals that $V_c \sqrt{D}$ is indeed constant to a remarkable extent. Table E-2 lists the present average results, with the projectile material. Considering the factors (see Appendix C discussion) which affect sensitivity for a given explosive, the present values appear reasonable.

The simplicity of Eqs. (E-2) and (E-3) can hardly be improved upon. However, the situation is more complex than it appears to be, particularly for noncircular or annular cross-sections. For the three such cases considered herein, it is worth noting that computing D_{eq} gave $V_c\sqrt{D}$ results consistent with the solid circular cross-sections (Table E-1). D_{eq} is the diameter of an equivalent circular area.

The critical area concept can obviously be employed to check the "D" computations. For example, the projectile cross-section area, A must be greater than A_{cr}. From a conservative point of view, the smallest dimension (W) of a rectangular projectile is the most important one from $U_{s_p}\ t_{cr}$ considerations. The example of the R(5 X 11) projectile in Appendix C illustrates this. Obviously, W must be greater than $2U_{s_p}\ t_{cr}$ or A_{cr} is zero and detonation initiation will not occur.

Table E-1. Determination of Explosive Sensitivity Coefficient.

$(V_c \sqrt{D} = \text{CONSTANT})$

EXPLOSIVE	PROJECTILE	D	V_c	$V_c\sqrt{D}$
~	~	mm	$\frac{mm}{\mu\text{-sec}}$	$\frac{mm^{3/2}}{\mu\text{-sec}}$
COMP-B3	C(5)	5.00	2.020	4.517
COMP-B3	R(5x11)	8.37*	1.415	4.093
COMP-B3	A(9x15)	13.65*	1.275	4.710
COMP-B3	C(10)	10.00	1.225	3.874
COMP-B3	A(5x15)	14.14*	1.105	4.155
COMP-B3	C(15)	15.00	1.000	3.873
				4.204av
COMP-B	C(6.35)	6.35	1.320	3.326
COMP-B	C(12.70)	12.70	0.900	3.207
COMP-B	C(14.94)	14.94	0.850	3.285
				3.27av
TNT	C(6.00)	6.00	0.770	1.886
TNT	C(7.50)	7.50	0.690	1.890
TNT	C(10.00)	10.00	0.599	1.894
TNT	C(12.00)	12.00	0.548	1.898
TNT	C(15.00)	15.00	0.492	1.906
				1.895av
TETRYL	C(3.175)	3.175	0.804	1.433
TETRYL	C(7.620)	7.620	0.541	1.493
TETRYL	C(12.700)	12.700	0.433	1.543
TETRYL	C(14.940)	14.940	0.387	1.496
				1.491av
PBX-9404	C(1.270)	1.270	2.20	2.479
PBX-9404	C(1.778)	1.778	1.62	2.160
PBX-9404	C(3.556)	3.556	1.13	2.130
PBX-9404	C(7.620)	7.620	0.75	2.070
PBX-9404	C(10.160)	10.160	0.65	2.072
PBX-9404	C(19.050)	19.050	0.50	2.182
				2.182av

NOTE: V_c (mm/μ-sec) = V_c (km/sec)

*D = square root of cross-section area times $2/\sqrt{\pi}$

= Equivalent Diameter, D_{eq}.

Table E-2. Explosive Sensitivity Coefficients (A).

EXPLOSIVE	PROJECTILE MATERIAL	A
~	~	$\frac{m^{3/2}}{\mu sec}$
~	~	PRESENT RESULTS
COMP-B3*	Steel (Ref. 2)	4.204
COMP-B	Steel and Brass (Ref. 6)	3.273
TNT (Pressed)	Copper (Ref. 8)	1.895
TETRYL (Porous)	Steel and Brass (Ref. 6)	1.491
PBX-9404	Steel (Ref. 1)	2.182**

*See comments in Appendix C with respect to this explosive.

**Reference 1 determined A to be 2.05, possibly by using all points defining the detonation threshold (including those just below the threshold).

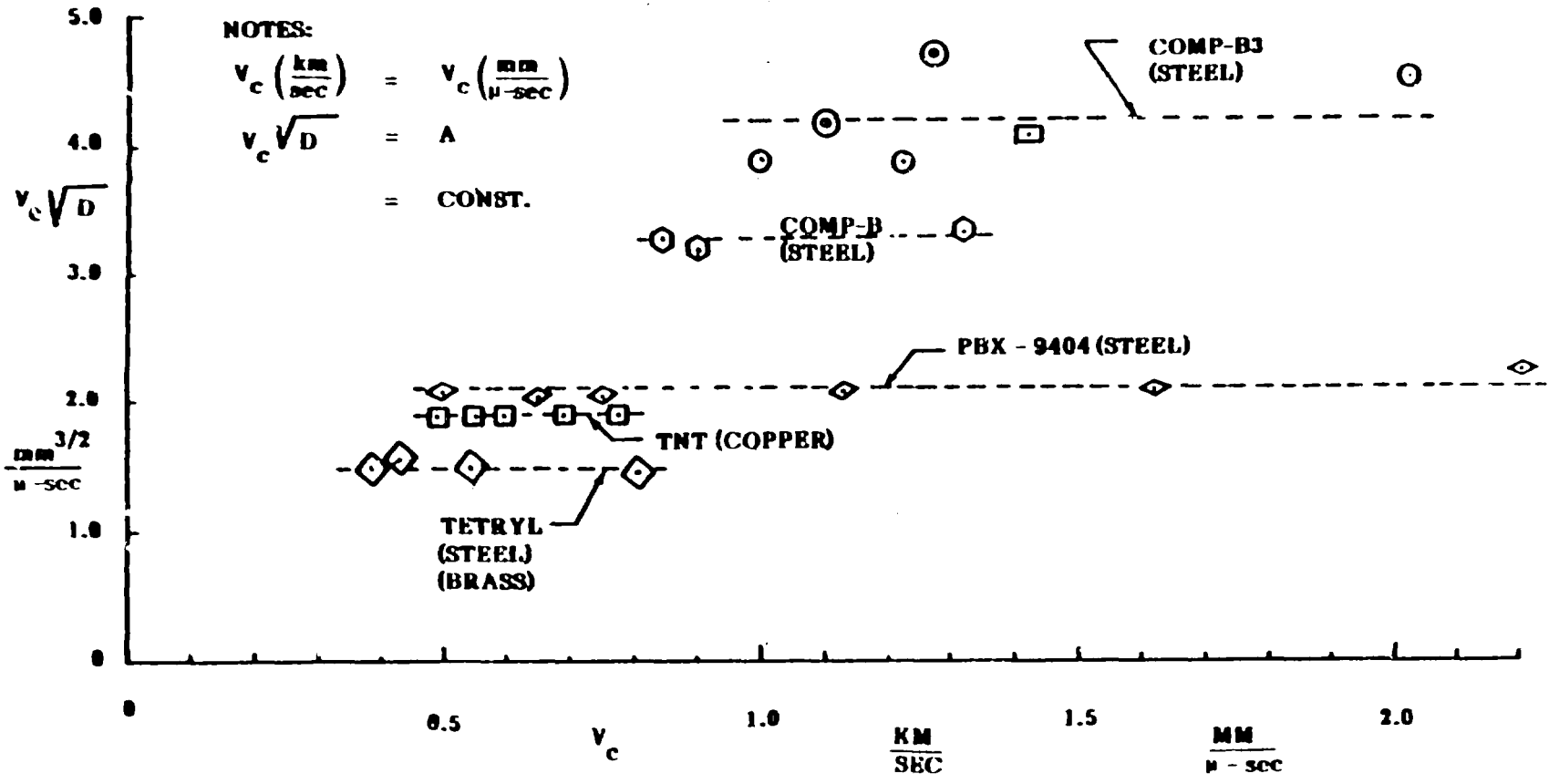

Figure E-1. $V_c\sqrt{D}$ versus V_c for five explosives.

APPENDIX F

DIAMETER EFFECT ON DETONATION SHOCK VELOCITY FOR CYLINDRICAL EXPLOSIVE SPECIMENS

It is well known that there is a size effect on the detonation velocity achieved in cylindrical explosive samples (for example, see [27]-[33]). That is, the final detonation velocity, D, achieved in a cylindrical explosive specimen (ignited on one end) is dependent on the diameter (d) of the sample. Normally, there is also a limiting small diameter such that detonation will not propagate (D = 0). Equation (1) of [29] is a rather general form of the observed relationships between D and d. This equation is:

$$\frac{D_\infty - D}{D_\infty} = f\left(\frac{RZL}{d_{ex}}\right) = \frac{\Delta D}{D_\infty} \qquad \text{(F-1)}$$

Where

D_∞ = Detonation shock velocity in an infinite explosive medium.

D = Detonation shock velocity in a cylindrical explosive sample whose diameter is d_{ex}.

d_{ex} = Diameter of explosive specimen.

RZL = Reaction Zone Length, or some characteristic length associated with the detonation phenomena.

The authors of [29] and [30] consider the reaction zone length to be:

$$RZL = (D - Up)\ tr \qquad \text{(F-2)}$$

Where

Up = Particle velocity in the reaction zone behind the detonation shock front.

t_r = Reaction time.

Thus Eq. (F-1) could be written as:

$$\frac{D_\infty - D}{D_\infty} = f\left[\frac{(D - Up)\ tr}{d_{ex}}\right] \qquad \text{(F-3)}$$

Where f still denotes a general functional relationship [31]. Both theoretical and experimental results for many explosives indicate that ΔD is directly proportional to $1/d_{ex}$ so that an explicit functional relationship is:

$$\frac{D_\infty - D}{D_\infty} = K\left[\frac{(D - Up)\ tr}{d_{ex}}\right] \qquad \text{(F-4)}$$

Where

K = A numerical constant.

Physical reasons for the size effect on the detonation velocity are stated by Kistiakowsky [27] and by Ubbelohde [28]. They say that if radial expansion occurs in a cylindrical charge behind the wave front before the chemical reactions have been completed, the chemical energy of this unreacted explosive is unavailable to drive the wave. The amount of radial expansion is governed by the diameter of the charge; the smaller the diameter, the greater the radial expansion and chemical energy loss. This chemical energy loss lowers the detonation shock velocity from D_∞ to D.

Table F-1 is a list of detonation shock information for the explosives analysed in this report. Sources for this information are given also. This information is from one-dimensional test results.

A question which naturally arises is: What relation does the phenomena, described above in this appendix, have to the topic of the main body of this report where the explosive samples are large enough (relative to the projectile size) to be considered an infinite medium?

A glance at Figure 1 (which is reasonably scaled) reveals that even though the explosive target is large relative to the projectile, the highly shocked critical region where the ignition reaction begins is confined to a volume whose dimensions are the same order as the projectile diameter. Generally, as shown herein (Tables 1 through 6), these dimensions are always less than the projectile diameter. In addition, digital simulations which model the molecular dynamics of two-dimensional impacted solids ([34] and [35] show that:

"Lateral transfer of shock energy is minimal, even when the lattices are initially thermally highly excited."

This is a direct quote from [35] and means that most of the shock effects are confined to the material immediately ahead of the finite projectile. Numerous figures in [34] and [35] illustrate this also.

Thus, it is not surprising that there is a strong projectile cross-section size effect on explosive detonation via impact. Furthermore, certain aspects of finite projectile induced detonation may be somewhat similar or analogous to certain features of the cylindrical explosive diameter effect as delineated above in this appendix.

Sufficient information was not available in [1], [2], [6], and [8] (or other sources) to ascertain if Eqs. (F-3) or (F-4) were applicble to the projectile induced detonation data specifically considered in this report. However, somewhat analogous to Eq. (F-2), an ignition zone length, IZL, could be computed as follows:

$$IZL = (U_{s_{ex}} - U_{p_{ex}})\, t_{cr} \qquad (F-5)$$

Where $U_{s_{ex}}$, $U_{p_{ex}}$ and t_{cr} have the same definitions employed in the main body of this report. See also Figure 1 which shows that this is the distance between the projectile and the shock front when $t = t_{cr}$. Ignition phenomena must occur within this length of shock compressed explosive material. Was there some relation between the IZL and the projectile cross-section dimensions?

To answer this question, the ratio, $IZL/\sqrt{A}$ was computed for all the data considered herein. A is the cross-section area of the projectile. It was found empirically that:

$$\frac{IZL}{\sqrt{A}} = \frac{(U_{s_{ex}} - U_{p_{ex}})\, t_{cr}}{\sqrt{A}} \qquad (F\text{-}6)$$

$$= C_5$$

C_5 is a constant or practically a constant, over a wide range of conditions for a given explosive. C_5 was different for each of the five explosives considered in this report. See Table 6 and Figures 6 and 7 in the main body of this report.

The ratio, $IZL/\sqrt{A}$, is somewhat analogous to the ratio, RZL/d_{ex}, on the RHS of Eqs. (F-1), (F-3), and (F-4). Equation (F-6) means that the IZL is directly proportional to the projectile cross-section area. Note that this result (Eq. (F-6)) was established independently of Moulard's Critical Area Concept.

TABLE F-1. Explosive Detonation Characteristics.

EXPLOSIVE	ρ_o	D_{CJ}	$U_{p_{CJ}}$	$P_{s_{CJ}}$
	$\frac{\text{Gram}}{\text{cm}^3}$	$\frac{\text{cm}}{\mu\text{-sec}}$	$\frac{\text{cm}}{\mu\text{-sec}}$	KBAR
COMP-B3	1.70	0.790 Ref. 12	0.280 Ref. 12	376
COMP-B	1.70	0.780 Refs. 12, 33	0.290 Ref. 12	385
TNT (Pressed)	1.54	0.690 Ref. 31	0.205 Ref. 26	219
TETRYL (Porous)	1.50	0.705 Ref. 13	~	~
PBX-9404	1.84	0.878 Refs. 26, 33	0.225 Ref. 26	360

APPENDIX G

MINIMUM DETONATION SHOCK VARIABLE MAGNITUDES VIA A CRYSTAL LATTICE FRACTURE CRITERION

From particle dynamics concepts, Fitzgerald ([46], Chapter III) derived an expression for the particle velocity necessary to produce self-sustained lattice disintegration. He called this velocity the phonon-fission velocity, V_f.

Consequently, it seemed feasible that lattice breakup could initiate detonation in explosives. If so, then V_f would be the minimum particle velocity (due to impact or shock) required to cause detonation in one-dimensional large samples. The corresponding shock velocity, U_{s_f} and shock pressure, P_{s_f}, are (Appendix A):

$$U_{s_f} = Co + S * V_f \qquad (G\text{-}1)$$

$$Ps_f = \rho o_{ex} * U_{s_f} * V_f \qquad (G\text{-}2)$$

Reference [47] documents the computation of Vs, U_{s_f} and P_{s_f} for Comp-B3, Comp-B, TNT, PBX-9404, and Tetryl. Available experimental data compared favorably with the computed results.

Table G-1 lists V_f, U_{s_f} and P_{s_f} for the above explosives [47]. The V_f magnitude for Tetryl (ρ_o = 1.5 grams/cc) is considered slightly high since certain elastic wave velocities (employed to compute V_f) were for ρ_o = 1.68 grams/cc.

Of particular interest in the present analysis were the magnitudes of U_{s_f} (Table G-1) which would be employed in Eq. (16) of Section II.C to compute an upper bound for $(\dot{E})_{t_{cr}}$. Table G-2 contains the numerical results for both the upper and lower bounds of $(\dot{E})_{t_{cr}}$ as per Eq. (16). These results are plotted, as appropriate, in Figures 12, 13, and 14. See the discussion in Section II.C.

For comparison purposes, experimental results for $P_{s_{min}}$ from the present analysis were acquired via Figures G-1 through G-5. In these figures the inverse projectile diameter (1/dp) is plotted versus the initial initiating pressure, Ps. True one-dimensional conditions are considered to exist where 1/dp equals zero.

Note that for these explosives:

$$(P_s - P_{s_{min}})\ dp \approx \text{Constant} \qquad (G\text{-}3)$$

$P_{s_{min}}$ is the extrapolated point where 1/dp equals zero, or one-dimensional conditions exist.

The computed P_{s_f} and experimental $P_{s_{min}}$ comparison varies from fair (TNT, Tetryl, and PBX-9404) to very good (Comp-B3 and Comp-B).

See also the theoretical and experimental results comparison presented in [47]. This illustrates that the magnitude of experimental $P_{s_{min}}$ data spread which exists for strictly one-dimensional test conditions is comparable to the differences in P_{s_f} and $P_{s_{min}}$ exhibited in Figures G-1 through G-5.

Equation G-3 implies that:

$$(P_s - P_{min}) \sqrt{A} = \text{Constant} \qquad \text{(G-4)}$$

and Eq. (G-4) multiplied by Eq. (6) (Section II.B) yields:

$$(P_s - P_{min}) (U_{s_{ex}} - U_{P_{ex}}) t_{cr} = \text{Constant} \qquad \text{(G-5)}$$

An analyses of the present sets of projectile-explosive impact detonation data has confirmed Eqs. (G-4) and (G-5) to a remarkable extent. See Section II.B in the main text of this report.

TABLE G-1. Numerical Results for V_f, U_{sf} and P_{sf}.

MATERIAL	V_f	U_{s_f}	P_{s_f}
~	$\frac{cm}{\mu-sec}$	$\frac{cm}{\mu-sec}$	KBARS
Comp-B3 $\rho_o = 1.70$	0.04170	0.3751	26.59
Comp-B $\rho_o = 1.70$	0.04077	0.3631	25.16
TNT (Pressed) $\rho_o = 1.635$	0.03739	0.2959	18.09
TETRYL* (Porous) $\rho_o \approx 1.50$	0.03543	0.1794	9.53
PBX-9404 $\rho_o = 1.835$	0.04109	0.3469	26.16

*V_f, U_{s_f} and P_{s_f} for Tetryl are slightly high since longitudinal (C_l) and transverse (C_t) wave velocity data for $\rho_o = 1.68$ gram/cc were employed to compute V_f [47].

TABLE G-2. Computation of Upper and Lower Bounds on $(\dot{E})_{t_{cr}}$.

EXPLOSIVE	C_2^2 TABLES 1-5	$\frac{C_2^2}{\rho_{o_{ex}}}$	u_{s_f} TABLE G-1	$\frac{C_2^2}{\rho_{o_{ex}} U_{s_f}}$	D_∞ TABLE F-1	$\frac{C_2^2}{\rho_{o_{ex}} D_\infty}$	P_{s_f} TABLE G-1
~	$\frac{\text{Joules}^2}{\text{CM}^4 \times 10^6}$	$\frac{\text{J-CM}}{(\mu\text{-sec})^2}$	$\frac{\text{CM}}{\mu\text{-sec}}$	$\frac{\text{Joules}}{\mu\text{-sec}}$	$\frac{\text{CM}}{\mu\text{-sec}}$	$\frac{\text{Joules}}{\mu\text{-sec}}$	KBARS
COMP-B3	41.5328	244.31	0.3751	651.32	0.7900	309.253	26.59
COMP-B	16.7690	98.641	0.3631	271.66	0.7800	126.463	25.16
TNT	0.2782	1.7012	0.2959	5.75	0.6900	2.466	18.086
TETRYL	0.2460	1.640	0.1793	9.15	0.705	2.326	9.53
PBX-9404	4.6708	25.454	0.3469	73.38	0.8780	28.937	26.16

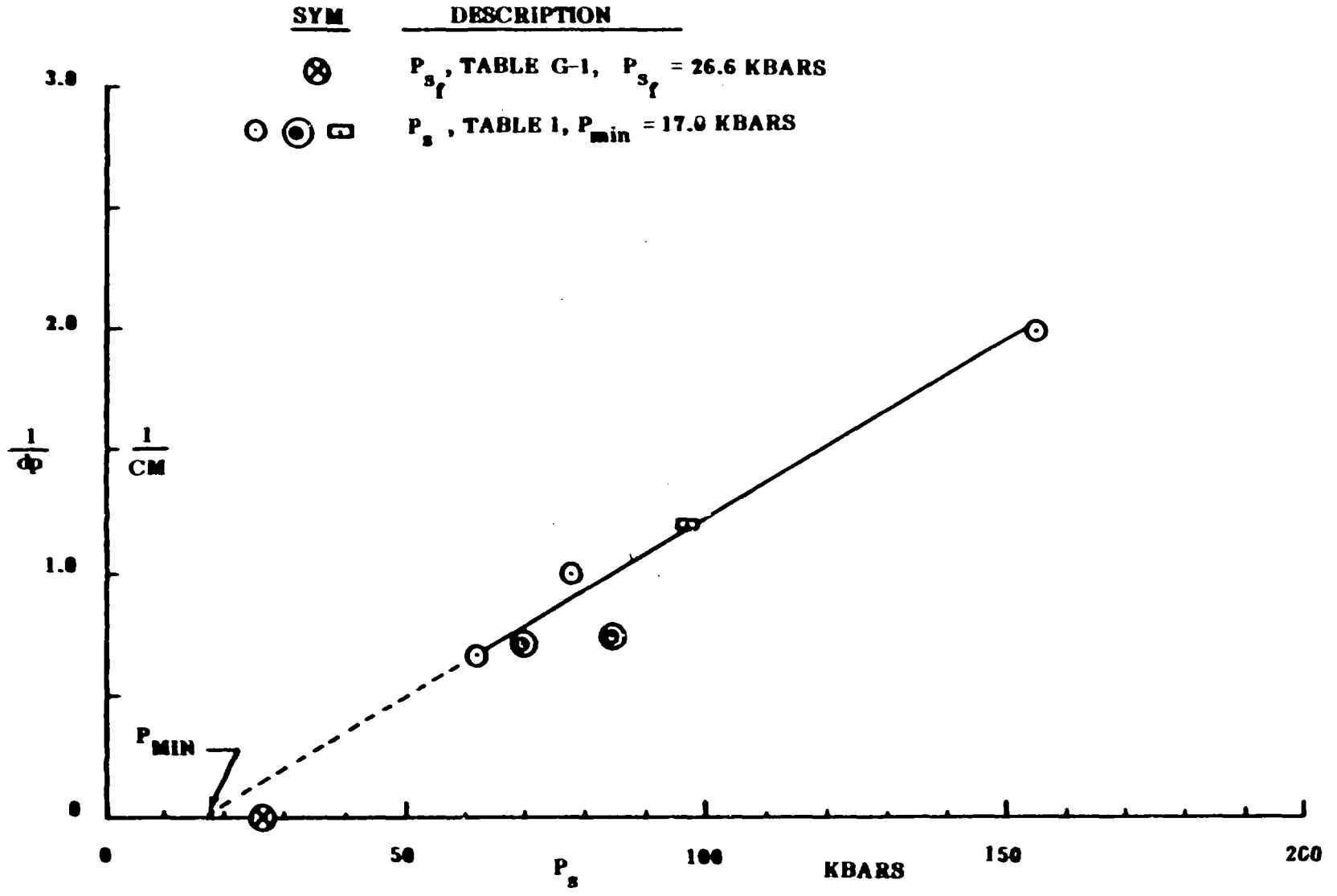

Figure G-1. Inverse projectile diameter versus impact shock pressure for Comp-B3.

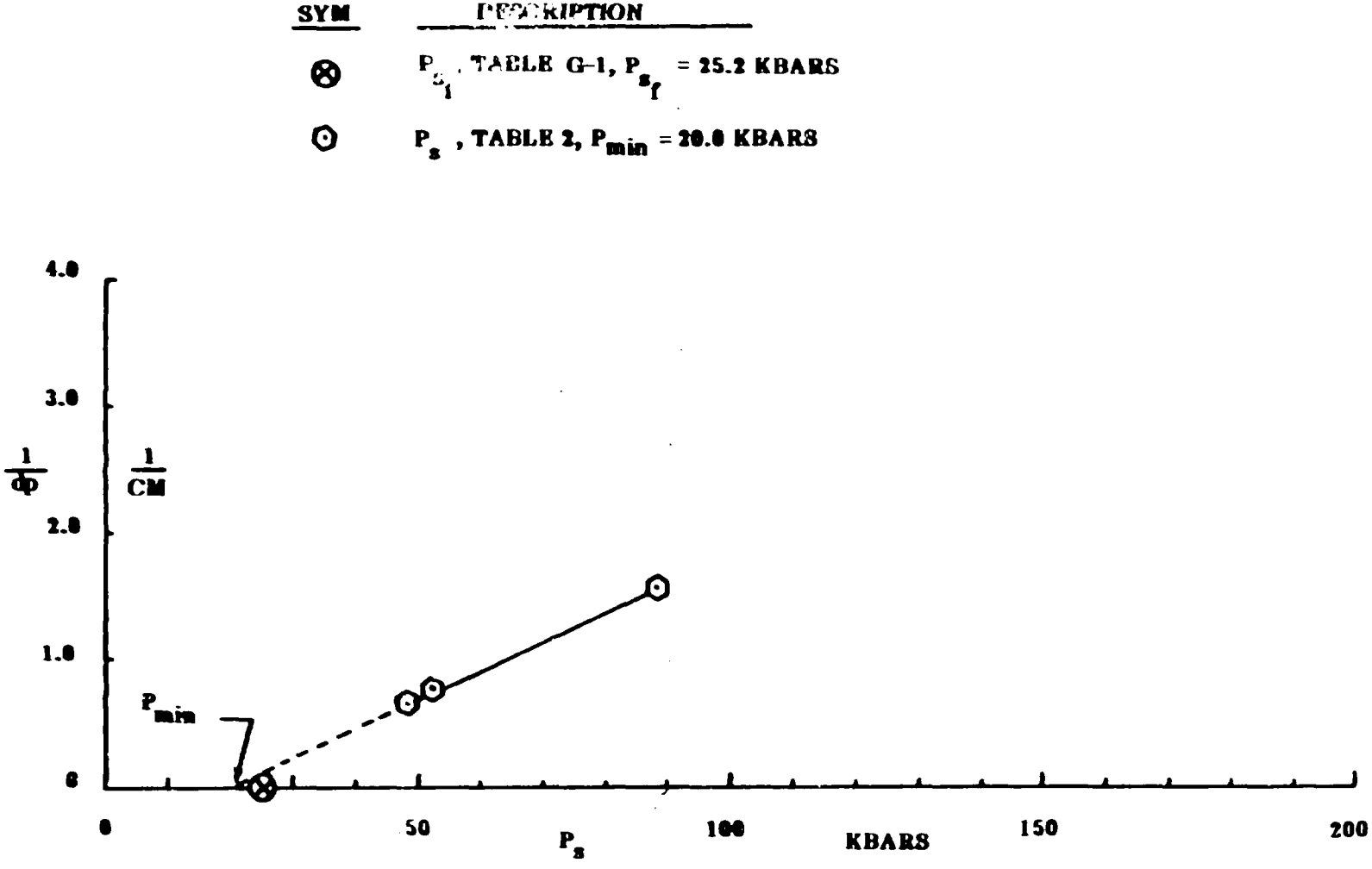

Figure G-2. Inverse projectile diameter versus impact shock pressure for Comp-B.

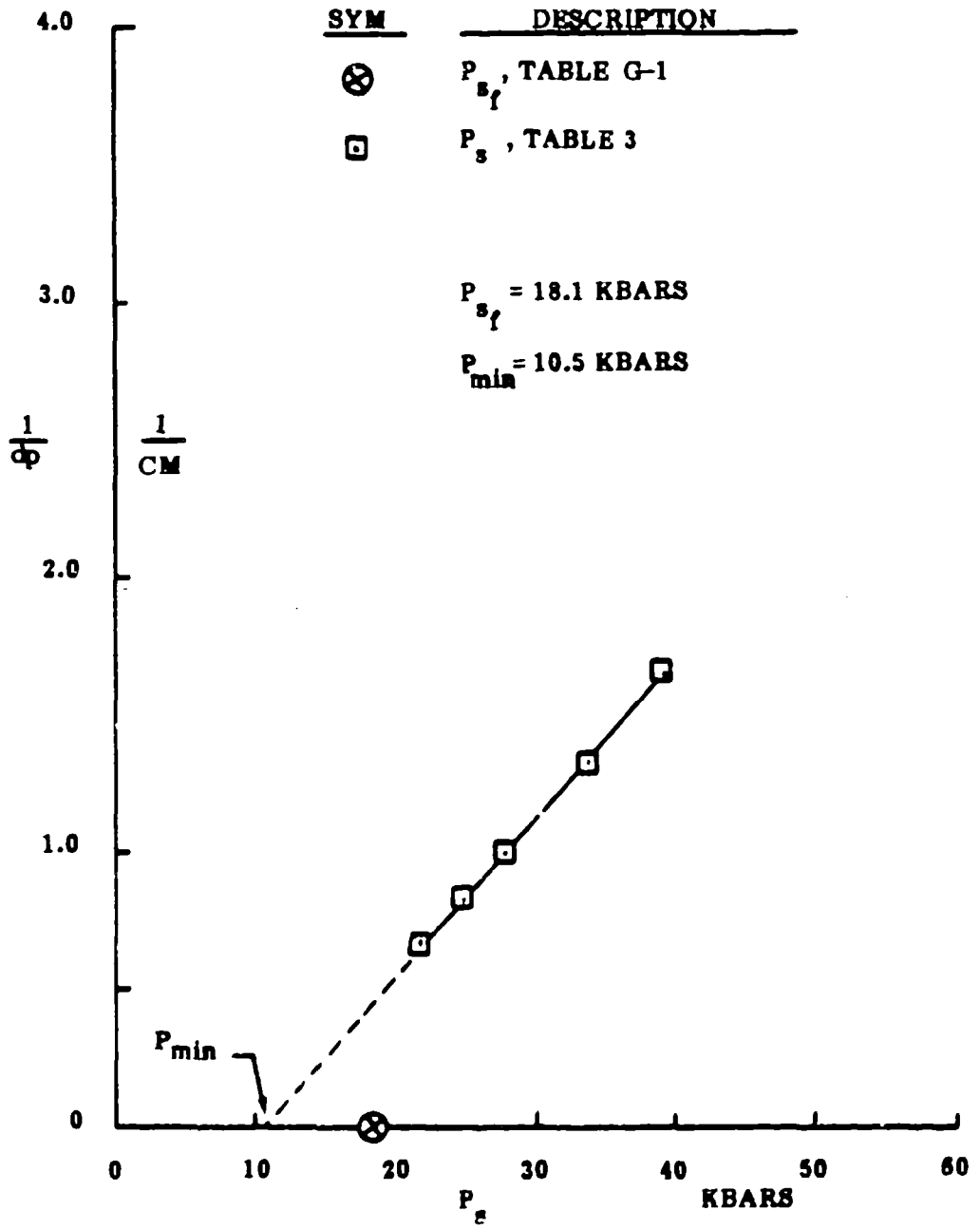

Figure G-3. Inverse projectile diameter versus impact shock pressure for TNT.

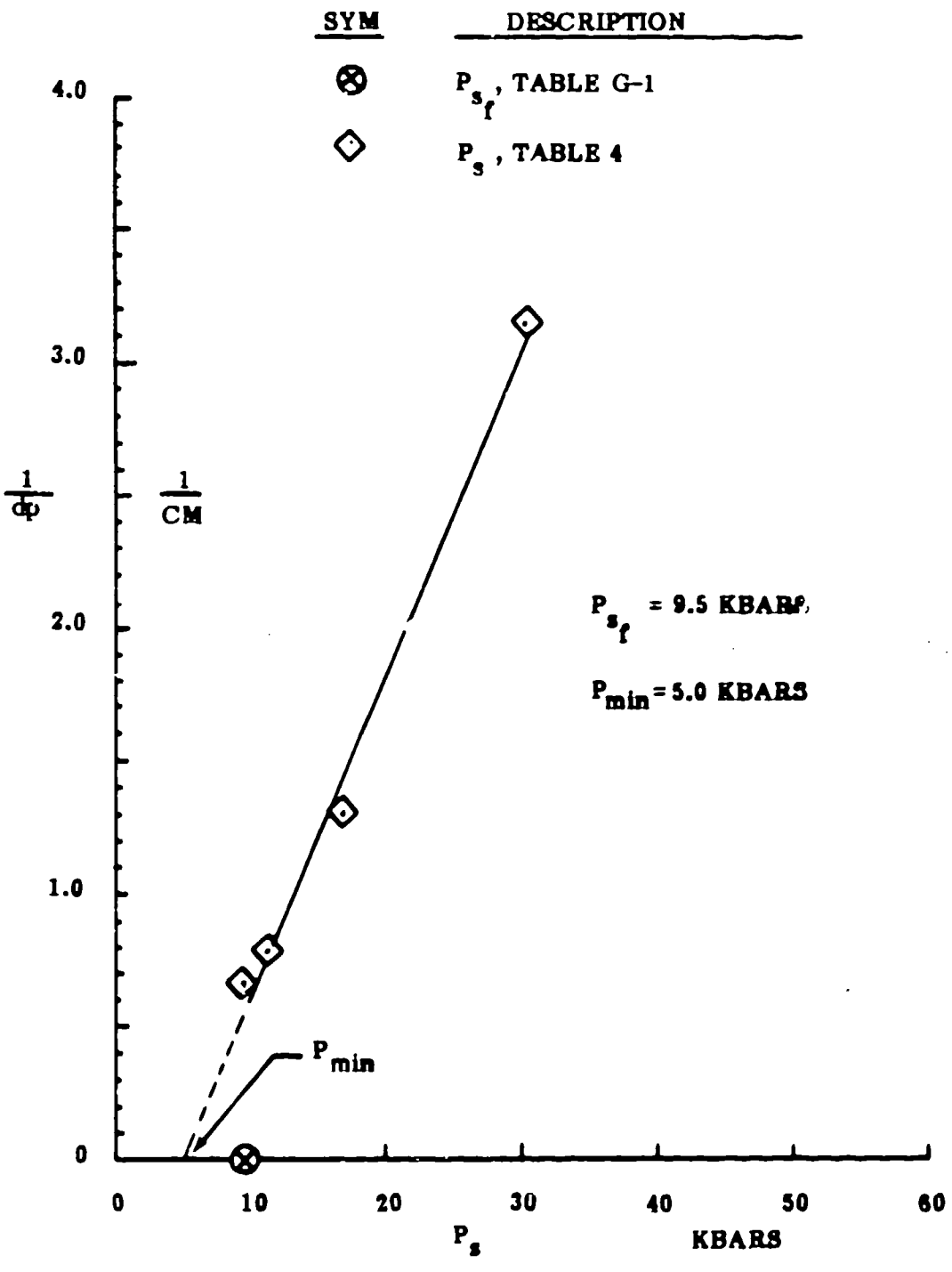

Figure G-4. Inverse projectile diameter versus impact shock pressure for Tetryl.

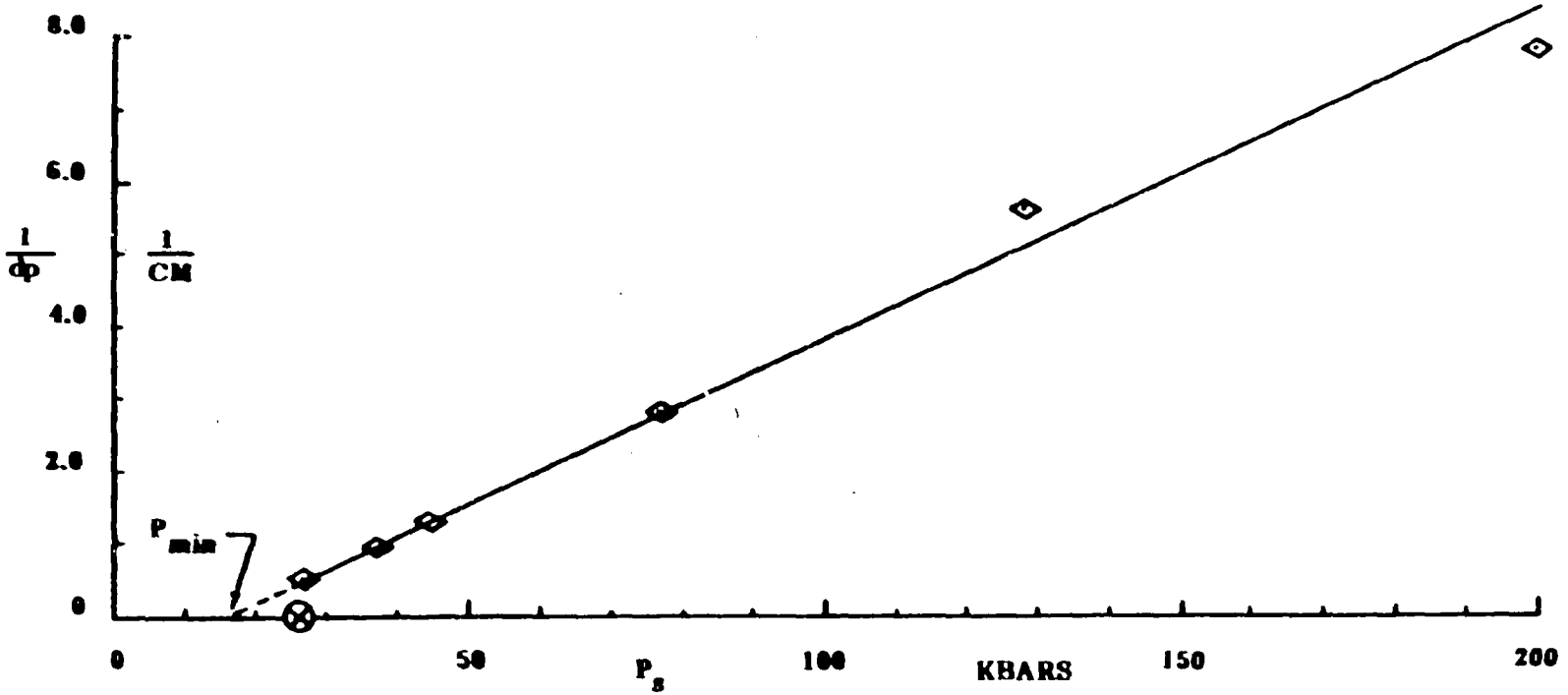

Figure G-5. Inverse projectile diameter versus impact shock pressure for PBX-9404.

DISTRIBUTION

	No. of Copies
Sandia National Laboratories ATTN: Dr. D. D. Bloomquist P. O. Box 5800 Division 1252 Albuqueque, NM 87185	3
Los Alamos National Laboratory ATTN: Dr. Steven A. Sheffield Group M-9 Mail Stop T-959 Los Alamos, NM 87545	3
Antiarmor Munitions Technical Office ATTN: AMCLO-AM, Dr. P. Howe Building 328 Aberdeen Proving Ground, MD 21005-5066	3
Explosives Effects Branch ATTN: SLCBR-TB-EE, Dr. R. Frey Aberdeen Proving Ground, MD 21005-5066	3
Los Alamos National Laboratory ATTN: Dr. I. E. Lindstrom Group WX-5 Mail Stop G-780 Box 1663 Los Alamos, NM 87545	3
Naval Surface Weapons Center ATTN: R12, Mr. J. M. Short White Oak Silver Spring, MD 20903-5000	3
Naval Surface Warfare Center ATTN: Mr. Tom Wasmund Code G-13 Dahlgren, VA 22448	3
Eglin Air Force Base ATTN: AD/CZL, Mr. Bill Dyess Eglin AFB, FL	1
Eglin Air Force Base ATTN: AD/ALJW, Dr. Joe Foster Eglin AFB, FL	2
U.S. Army Materiel Systems Analysis Activity ATTN: AMXSY-MP Aberdeen Proving Ground, MD 21005	1

	No. of Copies
IIT Research Institute ATTN: GACIAC Mr. A. J. Tulis 10 W. 35th Street Chicago, IL 60616	2
TASC ATTN: Mr. Charles E. Clucus 907 Mar-Walt Drive Fort Walton Beach, FL 32548	2
University of Alabama at Huntsville (UAH) Research Institute ATTN: Mr. C. L. Adams Dr. B. Z. Jenkins Huntsville, AL 35816	5 1
Johns Hopkins University ATTN: Professor E. R. Fitzgerald 127 Latrobe Hall 34th and Charles Street Baltimore, MD 21218	6
McGill University Department of Mechanical Engineering ATTN: Professor J. H. Lee 817 Sherbrooke West Montreal, Canada H3A 2K 6	3
University of Illinois Department of Aeronautical and Astronautical Engineering ATTN: Professor R. A. Strehlow Urbana, IL 61801	3
Franco - German Institute Saint Louis (ISL) ATTN: Mr. Henry P. A. Moulard 12 Rue De L'Industrie Saint Louis, France 68300	3
One Daniel Burnham Court ATTN: Dr. S. W. Yuan Apartment 1222 San Francisco, CA 94109	2

DISTRIBUTION (Concluded)

	No. of Copies
AMCPM-PA-JTMD, BG Capps	1
AMCPM-PA-SE, COL Flick	1
Mr. Don Adams	1
AMCPM-HA, COL Liberatore	1
AMCPM-HA-SE, Mr. James Harchanko	1
AMCPEO-CM, Mr. Jerry Brown	1
AMSMI-RD, Dr. McCorkle	1
Dr. Rhoades	1
Dr. Stephens	1
AMSMI-RD-RE, Dr. R. L. Hartman	1
AMSMI-RD-SS, Dr. Grider	1
Mr. Davis	1
AMSMI-RD-SS-SE, Mr. Grabney	1
Mr. Jordan	1
Mr. Grabney	1
Mr. Waddle	1
AMSMI-RD-SS-AA, Dr. Billingsley	10
Mr. Head	1
Dr. Oliver	1
Mr. Harris	1
AMSMI-RD-ST-WF, Mr. Schexnayder	1
Mr. Lovelace	I
Mr. Lienau	1
Ms. Brantley	1
Mr. Hill	1
Mr. Cornelius	1
Mr. MacDonald	1
AMSMI-RD-RE, Mr. Jennings	3
AMSMI-RD-PR, Dr. Wharton	3
AMSMI-RD-CS-R	5
AMSMI-RD-CS-T	1
AMSMI-GC-IP, Mr. Fred Bush	1